Transactions of Tianjin University (2022) 28:33–52
https://doi.org/10.1007/s12209-021-00303-w

REVIEW

Visible Light-Responsive N-Doped TiO_2 Photocatalysis: Synthesis, Characterizations, and Applications

Shiwen Du[1] · Juhong Lian[1] · Fuxiang Zhang[1]

Received: 10 May 2021 / Revised: 18 June 2021 / Accepted: 21 June 2021 / Published online: 29 July 2021

Abstract

Photocatalysis based on semiconductors has recently been receiving considerable research interest because of its extensive applications in environmental remediation and renewable energy generation. Various semiconductor-based materials that are vital to solar energy utilization have been extensively investigated, among which titanium oxide (TiO_2) has attracted considerable attention because of its exceptional physicochemical characteristics. However, the sluggish responsiveness to visible light in the solar spectrum and the inefficient separation of photoinduced electron–hole pairs hamper the practical application of TiO_2 materials. To overcome the aforementioned serious drawbacks of TiO_2, numerous strategies, such as doping with foreign atoms, particularly nitrogen (N), have been improved in the past few decades. This review aims to provide a comprehensive update and description of the recent developments of N-doped TiO_2 materials for visible light-responsive photocatalysis, such as (1) the preparation of N-doped/co-doped TiO_2 photocatalysts and (2) mechanistic studies on the reasons for visible light response. Furthermore, the most recent and significant advances in the field of solar energy applications of modified N-doped TiO_2 are summarized. The analysis indicated the critical need for further development of these types of materials for the solar-to-energy conversion, particularly for water splitting purposes.

Keywords N-doped TiO_2 · Visible light-responsive · Photocatalysis · Solar energy

Introduction

Developing advanced photocatalysts for large-scale solar energy conversion systems is an effective method to alleviate the increasing energy demand and environmental degradation issues. Since the pioneering work conducted by Fujishima and Honda in 1972 [1], who developed n-type rutile titanium oxide (TiO_2) for photoelectrochemical water splitting under light illumination, the use of semiconductor-based materials for photocatalysis has become a promising technology to convert inexhaustible solar energy into storable chemical energy. In the past few decades, numerous candidate semiconductor materials, such as TiO_2, CdS, and C_3N_4, have been developed and utilized as photocatalysts and extensively investigated. Among these numerous photocatalysts, TiO_2 has attracted considerable attention because of its high photochemical stability, environmental friendliness, cost-effectiveness, and other excellent properties [2, 3].

In nature, TiO_2 has eight types of crystal structures, namely, anatase, rutile, brookite, TiO_2–H, TiO_2–II, TiO_2–III, TiO_2–R, and TiO_2–B [4]. Among them, only the first three types of crystal phases have been investigated, mostly for application purposes, because these titanium oxides can be naturally formed at atmospheric pressure. The structural parameters and schematic structures of the three structures are illustrated in Fig. 1 and Table 1, respectively. Figure 1 shows that, in all of the three crystalline structures of TiO_2, titanium (Ti) atoms are sixfold coordinated to oxygen (O) atoms, forming the distorted TiO_6 octahedral structure [5]. Despite having similar constituent structural units, their physical properties are different: Rutile TiO_2 is the most thermodynamically stable phase, whereas the metastable phase of anatase and brookite TiO_2 can be transformed into the rutile phase after calcination at a certain temperature. In general, both rutile and anatase TiO_2 have a tetragonal structure, whereas brookite TiO_2 has an orthorhombic structure (as shown in Table 1). These differences in the crystallite parameters of TiO_2 with different crystal phases can result

✉ Fuxiang Zhang
fxzhang@dicp.ac.cn

[1] State Key Laboratory of Catalysis, iChEM, Dalian Institute of Chemical Physics, Chinese Academy of Sciences, Dalian National Laboratory for Clean Energy, Dalian 116023, China

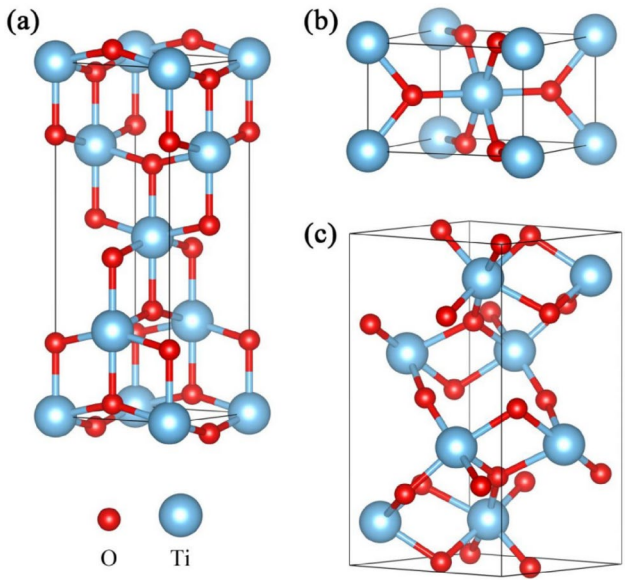

Fig. 1 Crystal configurations of **a** anatase, **b** rutile, and **c** brookite TiO_2. The small red sphere and large blue sphere represent the O and Ti atoms, respectively

in different electronic structures and physicochemical properties of TiO_2, which further leads to different activities in photocatalytic reactions. For instance, anatase TiO_2 shows higher water reduction activity than rutile TiO_2, whereas rutile TiO_2 exhibits better water oxidation activity than anatase TiO_2 [6]. At the same time, compared with anatase and rutile TiO_2, brookite TiO_2 shows better performance in several photocatalytic reactions [7]. These differences in the application of photocatalysis originate from not only the differences in physicochemical properties caused by physical structures but also the differences in electronic structures.

Density functional theory simulations revealed that the calculated bandgap for anatase, rutile, and brookite TiO_2 (as shown in Fig. 2) ranges from 1.86 to 2.38 eV [9], which are smaller than the experimental values. These underestimations can be attributed to the fact that the generalized gradient approximation function usually underestimates the bandgap of semiconductors [10]. Moreover, anatase TiO_2 can be considered an indirect bandgap material, whereas rutile and brookite TiO_2 can be considered direct bandgap materials. In the electronic structures of the three types of TiO_2, the top of the valence band (VB) is primarily composed of O 2*p* orbitals and a few Ti 3*d* orbitals, whereas the bottom of the conduction band (CB) is primarily composed of Ti 3*d* orbitals and a few hybrid O 2*p* orbitals. Therefore, under light irradiation, the electrons are excited from the O 2*p* orbitals in the VB to the Ti 3*d* orbitals in the CB of the TiO_2 semiconductor, leaving the holes in the VB. Subsequently, these charge carriers migrate to the surface of the catalyst and participate in the corresponding redox reactions.

However, because of its wide bandgap (approximately 3.2 eV), TiO_2 can only utilize ultraviolet (UV) light, which accounts for only approximately 5% of solar energy reaching the Earth [11], for photocatalytic reactions. To overcome the poor light response of TiO_2 photocatalyst, diverse strategies, such as introducing oxygen vacancies (OVs) [12, 13], sensitizing with dyes [14, 15], utilizing the surface plasmon resonance effect on metals [16, 17], and tuning the bandgap by heteroatom doping [18, 19], have been implemented. Among these strategies, substituting the host anion and/or cation in the TiO_2 crystal lattice with various heteroatoms has been proven to be one of the most efficient routes to facilitate the utilization of visible light of TiO_2. Notably, ascertaining the most suitable impurity elements is the key step because foreign elements may disrupt the local chemical environment and charge balance in the TiO_2 matrix, such as the ionic radii and/or valence state deviations between the host anion and/or cation and the foreign element [20]. Thus far, cation dopants (such as transition metals [21–28], inner transition metals [29–32], and noble metals [33–35]), anion dopants (such as boron (B) [36, 37], carbon (C) [38, 39], nitrogen (N) [40, 41], fluorine (F) [42, 43], sulfur (S) [44, 45], and chlorine (Cl) [46, 47]), cation/anion co-dopants [48–51], and anion/anion co-dopants [52–54] have been utilized to adjust the optical and electrical properties of TiO_2 photocatalysts.

Extensive works on metal cation doping of TiO_2 photocatalysts have been reported. These reports show that metal cation doping can create an energy level of donor level (i.e., the level higher than the original VB maximum) or acceptor level (i.e., the level lower than the original CB minimum) in the forbidden bandgap of TiO_2, hence decreasing the bandgap and increasing the visible light sensitivity of TiO_2. However, doping of metal cation can decrease the carrier mobility, which is the result of the generation of strongly localized *d* states in the bandgap [55], and generate the electron–hole recombination centers derived from the newly inserted energy level [56], thus leading to the significantly

Table 1 Structural data for anatase, rutile, and brookite TiO_2 [8]

Structure	Crystal system	Space group	Group number	Cell parameters (Å)		
				a	*b*	*c*
Anatase	Tetragonal	$I4_1/amd$	141	3.758	3.758	9.514
Rutile	Tetragonal	$P4_2/mnm$	136	4.584	4.584	2.953
Brookite	Rhombohedral	*Pbca*	61	9.166	5.436	5.135

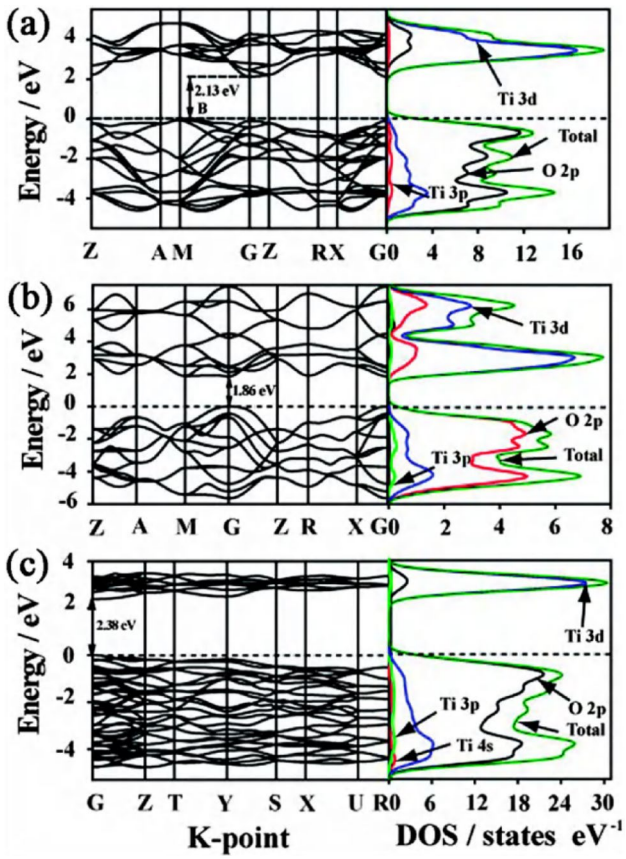

Fig. 2 Band structure and density of states of **a** anatase, **b** rutile, and **c** brookite TiO_2 (the Fermi level is set to 0). Reproduced from Ref. [9] with permission. Copyright 2014, Royal Society of Chemistry

reduced the photocatalytic performance. Moreover, the thermodynamic instability of the resulting cation-doped structure can cause photocorrosion in the photocatalysis process [57], which also hinders the practical application of TiO_2 photocatalysts.

By contrast, the use of nonmetal elements instead of metal elements to dope the TiO_2 semiconductor is a feasible pathway to develop its visible light activity. Since the breakthrough work conducted by Asahi et al. [58], who first investigated the visible light-driven catalytic performance of N-doped TiO_2 for the photodegradation of methylene blue and gaseous acetaldehyde, the nonmetal elements that act as dopants have been extensively investigated. Among these various nonmetal dopants (e.g., B, C, N, F, S, and Cl), the synthesis of N-doped TiO_2 has become the focus of considerable research because of the similar structural characteristics of O and N, such as polarizability, electronegativity, and ionic radii [56].

Thus far, an increasing number of literature reviews on the utilization of TiO_2 for solar energy utilization have been reported [59–64]. For example, Ma et al. [59] focused on the strategies to improve the generation of H_2 and the photoreduction of CO_2 with H_2O to other energy resources on TiO_2-based catalysts. They also summarized the studies of the charge carriers properties of TiO_2 to better understand the dynamic characteristics of TiO_2 photocatalysts with different phases. Ullattil et al. [60] focused on the various synthetic routes, structures, morphological changes, and electronic structures of black TiO_2 nanomaterials and provided readers an overview of the different applications of black TiO_2 nanomaterials in the field of environmental technology. Along similar lines, Naldoni et al. [64] illustrated the basic concepts of effective design of reduced TiO_2 photocatalysts for H_2 generation. Kumaravel et al. [61] and Chen et al. [62] discussed six unique challenges that inhibit the application of TiO_2 in organic effluents. Nonetheless, these reviews ignored the important role and the recent progress of visible light-responsive TiO_2 in practical applications in indoor environments, particularly the N-doped TiO_2, which has attracted considerable attention in visible light applications. Therefore, this review critically analyzes the improvement of visible light-sensitive N-doped TiO_2 photocatalysts. Moreover, the application prospect of these photocatalysts under visible light illumination, particularly the overall photocatalytic water splitting reaction, is reviewed.

Synthesis of N-Doped TiO_2

The key to the successful utilization of N-doped TiO_2 is to rationally select the synthesis strategies to prepare the target photocatalysts. Figure 3 shows the common methods involved in the synthesis of N-doped TiO_2 material. Based on the phase of the reactants, the strategies to prepare N-doped TiO_2 can be coarsely split into the wet chemistry and solid-phase methods.

Wet Chemistry Method

The wet chemistry method is a kind of strategy to prepare the target material through a chemical reaction with the participation of liquid, including the precipitation, hydrothermal, sol–gel, and electrochemical deposition methods. The sol–gel and hydrothermal methods are usually described as soft methods for doping N and/or other dopants into the TiO_2 crystal lattice, followed by calcination of the sample at high temperature. These methods usually have the advantages of being cleanroom-free, cost-efficient, and widely applicable. For this purpose, in a typical procedure, the doped N usually originates from nitric acid (HNO_3) [65, 66], ammonium hydroxide (NH_4OH) [67], urea (CH_4N_2O) [68, 69], ammonium chloride (NH_4Cl) [70, 71], and triethylamine (TEA) [72, 73] and the Ti precursors usually include titanium trichloride ($TiCl_3$) [74], titanium tetrachloride ($TiCl_4$) [75], titanium sulfate ($Ti(SO_4)_2$) [76], and titanium (IV)

Fig. 3 Common methods for the preparation of N-doped TiO_2

isopropoxide (TTIP) [77]. For example, Zhang et al. [65] selected HNO_3 as the N source and prepared nanocrystalline N-doped TiO_2 via a one-step solvothermal route with a low temperature (180 °C). In another effort, Panda's group [67] prepared N-doped yellow TiO_2 hollow spheres through a simple solvothermal method using aqueous titanium peroxocarbonate complex solution and NH_4OH as doping N sources. Notably, the catalytic activity of the obtained N–TiO_2 hollow spheres was better than that of other reported N–TiO_2 samples with different morphologies, which may be owing to the increased surface area and microreactor environment and the decreased recombination for light scattering caused by the inner hollow structure. By adding ammonia water, Cheng et al. [78] synthesized N-doped TiO_2 through a simple solution-based strategy. Their results showed that N doping could not only effectively inhibit the phase transition of TiO_2 from anatase to brookite but also help enhance the visible light absorption. Marques et al. [68] noted that the specific surface area and photocatalytic performance of N-doped TiO_2 could be influenced by different synthesis methods and parameters, e.g., doping temperature and molar ratio of urea to TiO_2. Di Camillo et al. [70] reported that N-doped TiO_2 nanofibers could be easily deposited via the electrospinning method. Their results showed that the light absorption properties of these nanofibers could be modified even with a small amount of N, which can result in good photocatalytic performance even when illuminated with visible light. Generally, the catalysts obtained by these methods have specific sizes and morphologies and usually exhibit a higher purity and uniformity. However, the extensive applications of the catalysts may be limited by the multistep synthesis process and inevitable use of organic solvents.

Solid-Phase Method

The solid-phase method is the thermal treatment process after mixing the N and TiO_2 sources under a given atmosphere. The solid-phase method is an economical and effective strategy for the large-scale synthesis of N-doped TiO_2. In addition to the ball milling, atomic layer deposition (ALD), and chemical vapor deposition methods (as shown in Fig. 3), the most common and efficient method used to prepare the target N–TiO_2 catalyst is to oxidize TiN powder under O_2 gas flow or nitrate TiO_2 powder under NH_3 gas flow [79]. A previous study reported that, by annealing at 200–550 °C for 1.5 h, the TiN sample could be converted into N-doped TiO_2 under an O_2 gas atmosphere. In their study, Morikawa et al. [80] determined that the calcination temperature can influence the crystal phase of the obtained sample. For instance, a homogeneous rutile phase could be obtained under the calcination temperature of 550 °C, whereas a small amount of TiN remained in the rutile phase of the TiO_2 sample under the calcination temperature of 400 °C. In another effort, Zhao's group [81] prepared N-doped TiO_2 samples with a mixed phase of anatase and rutile by the incomplete oxidation of TiN at various temperatures. Then, they investigated the photocatalytic performances of the obtained samples by photocatalytic degradation of gas-phase toluene under visible light illumination and achieved improved photocatalytic performances. Recently, Xia et al. [82] prepared highly ordered porous nanotube arrays of N-doped TiO_2 through oxidation of the preprepared porous TiN nanotube arrays in an air atmosphere. Photocatalytic investigations indicated that the obtained porous N-doped TiO_2 nanotube arrays had a visible light photocatalytic kinetic rate constant that was threefold larger than that of pure anatase TiO_2 nanotube arrays, which could be attributed to its higher visible light responsiveness and larger surface area.

As for the nitrification of the TiO_2 sample under an NH_3 gas atmosphere, the synthesis conditions have obvious effects on the morphology of the N-doped TiO_2 photocatalyst. Hashimoto's group [83] processed TiO_2 with anatase phase at different temperatures for 3 h under a mixed NH_3/Ar (67%/33%) gas flow to obtain the anatase phase of the N-doped TiO_2 material. The resulting samples with different colors signified that the change in calcination temperature and NH_3 gas flow resulted in different amounts of N in the N-doped TiO_2 material, which would result in different quantum yields because of the varying visible light absorption capabilities. In another effort, Pulgarin's group [84] used thiourea as the N source and mixed it with commercial anatase TiO_2 powder, followed by annealing at 400 °C and 500 °C, which resulted in visible light absorption of TiO_2.

Fang et al. [85] prepared N-doped TiO_2 by annealing P25 or TiO_2 xerogel powder under NH_3/Ar atmosphere at different temperatures. They determined that, compared with the N-doped TiO_2 prepared by annealing P25, the N-doped xerogel powder had a higher concentration of substituted N and exhibited a more distinct visible light absorption. Another study of N-doped TiO_2 with abundant OVs reported by Huang et al. [86], which was prepared by a facile hydrothermal method with a baking process in an NH_3 atmosphere, showed that more OVs could be generated by doping N into TiO_2, consequently ameliorating their catalytic behavior, particularly that of the OVs derived from visible light illumination.

Meanwhile, different N-containing molecules, such as urea and hexamethylenetetramine, were utilized for the doping process using a solid-phase (mechanochemical) method [68, 87]. In this process, the mixture containing TiO_2 and urea/hexamethylenetetramine was ground using a planetary ball mill and calcined at 400 °C to remove the residual organic substances. Notably, the obtained N-doped powder mainly consists of rutile TiO_2, indicating that high mechanical energy accelerates the phase transformation of anatase into rutile.

Furthermore, the sputtering process, ALD, and pulsed laser deposition are the most advanced techniques for the fabrication of crystalline N-doped TiO_2 thin films. For example, via the ALD operation, Vasu et al. [88] grew p-type epitaxial N-doped anatase TiO_2 (001) thin films on *c*-axis Al_2O_3 substrate, employing $TiCl_4$, double-distilled water, and NH_3 as Ti, O, and N sources, respectively. Their results showed the enhanced hole concentration and mobility of the obtained samples.

In each case, the presence of N within the lattice of TiO_2 has been shown to have an obvious effect on photocatalysis. As exhibited in Fig. 4 (Curve a), the pure anatase TiO_2 shows a single sharp edge, whereas the N-doped TiO_2 (Curve b in Fig. 4) shows two absorption edges: One is the main edge that originated from the oxide at approximately 390 nm, which does not change significantly compared with that of the undoped sample, and the other is the weak shoulder absorption at 400–550 nm wavelength. This noticeable shift of absorption to the visible light region corresponds to the yellow characteristic observed in the obtained N-doped samples [89]. Furthermore, with the increase in N content in the N-doped TiO_2, the shoulder absorption initially shifts to the lower energy region, indicating that the N-doped samples are sensitive to visible light. Although the shoulder absorption expands the light absorption of the obtained TiO_2 semiconductor to a certain extent, it cannot extend its intrinsic band absorption to the visible light range, which will result in the low visible light absorption efficiency of the prepared N-doped TiO_2. More importantly, this N substitution in TiO_2 usually leads to the generation of OVs, which results in a

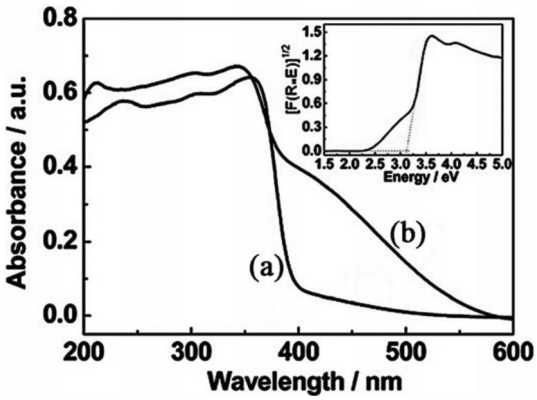

Fig. 4 UV–Vis diffuse reflectance (**a** pure anatase TiO_2, **b** N-doped TiO_2). Reproduced from Ref. [89] with permission. Copyright 2009, American Chemical Society

decrease in photocatalytic activity [90]. Hence, finding a simple and superior method for the scalable preparation of N-doped TiO_2 material with high visible light absorption efficiency is still a challenge.

Co-incorporation of N and other nonmetal anions has been considered a new potential pathway to construct the energy band structure of TiO_2. The remarkable synergetic effects in N,F-co-doped TiO_2 have been reported by some interesting works. For instance, Domen's group [91] utilized SiO_2 powder as the O source in their investigation of N,F co-doping into anatase TiO_2 by nitriding an $(NH_4)_2TiF_6$ precursor. Despite their results showing good absorption in the visible region ($\lambda < 570$ nm), which drives water oxidation for the N-doped catalyst, a shortcoming remains, i.e., under the preparation conditions, the N, O, and F contents of the product were uncontrollable. Afterward, Maeda et al. [92] prepared high-crystallinity $TiN_xO_yF_z$ material with an anatase crystal structure via nitridation of NH_4TiOF_3 in an NH_3 atmosphere, which can be used as a visible light-responsive photocatalyst for water oxidation at wavelengths of up to 540 nm. In another investigation, Zong et al. [93] reported that the visible light-responsive anatase TiO_2 platelets dominated by (001) facets were prepared by simple nitridation of the $TiOF_2$ precursor. The synthesized TiOFN materials exhibited excellent visible light-driven activity for water oxidation. Although the aforementioned studies achieved the absorption of visible light for N-doped TiO_2, it was only used in water oxidation, and the performance of water reduction for H_2 evolution of the catalyst was not investigated. Recently, Maeda and colleagues [94] fabricated a novel N,F-co-doped rutile TiO_2 by nitridation of the rutile TiO_2 and $(NH_4)_2TiF_6$ mixture and evaluated its photocatalytic oxidation activity of water. Their evaluation indicated that the N,F-co-doped samples exhibited water oxidation activity even in the presence of reversible electron acceptors under the action of the RuO_2 cocatalyst. Moreover, in

the presence of a shuttle redox mediator, the mixture of Ru/$SrTiO_3$:Rh and N,F-co-doped TiO_2 samples was used to obtain stoichiometric H_2 and O_2 without significant active degradation under visible light illumination.

In addition to the F dopant, B was selected as the co-dopant of N to optimize the band structure of the TiO_2 semiconductor. Liu et al. [95] reported the first example and demonstrated the substantial effect of B,N co-doping on improving the visible light response and charge carriers separation of TiO_2. Their results also indicated that, during the N doping process, the presence of the B dopant stabilized the structure relative to undoped TiO_2. Recently, in the study conducted by Hong et al. [96], a red anatase TiO_2 with a spatially homogeneous distribution of B and N dopants, which was sensitive to the sharp-edged strong visible light absorption spectrum over 680 nm, was obtained. The synthesized red TiO_2 sample can drive photocatalytic water oxidation for O_2 evolution under the illumination of visible light exceeding 550 nm and induce photocatalytic water reduction for H_2 evolution under visible light illumination. They concluded that the adsorption of HNCO and related derivatives on the surface of TiO_2 released by the thermal hydrolysis of urea significantly promoted the diffusion of the N dopant into the microspheres, thereby inducing uniform N doping with the help of the B dopant, resulting in a strong band-to-band absorption in the entire visible light range. Furthermore, several N-doped TiO_2 nanomaterials modified with other nonmetals (such as C, P, and S) were investigated for their visible light catalytic activities [97–99]. The results showed that, compared with undoped TiO_2 or mono-N-doped TiO_2, the modified N-doped TiO_2 samples exhibited enhanced photocatalytic activities.

Mechanisms for Visible Light Response

Generally, electron–hole pairs generated via light illumination are the basic components for photocatalytic reactions. Since the pioneering work conducted by Asahi et al. [58] to synthesize N-doped TiO_2 material by sputter deposition, tremendous efforts have been exerted to investigate the potential mechanisms for the photocatalytic reactions of N-doped TiO_2 particles under visible light illumination and explore the electronic, optical, and structural characteristics of N-doped TiO_2 samples.

Even though the visible light absorption and enhanced photocatalytic activity of N-doped TiO_2 catalysts have been generally recognized, in theory, there are still open debates about the chemical properties, location of the photoactive N species involved, and origin of the visible light response. In general, the main proposed mechanisms for the improved visible light absorption of N-doped TiO_2 can be divided into three areas, which are discussed in the subsequent paragraphs.

Based on the first principle calculations, in 2001, Asahi et al. [58] investigated the contribution of N doping to the narrowed bandgap of TiO_2 and compared three N-doped TiO_2 systems, namely, substitutional N doping, interstitial N doping, and both types of doping into anatase TiO_2. Their results indicated that the N 2*p* state could hybridize with the O 2*p* state (Fig. 5a), resulting in the narrowed bandgap and enhanced visible light-driven photoactivity. However, since 2003, this conclusion was challenged by other opinions, which tend to support that N doping will not result in the reduction of the TiO_2 semiconductor bandgap based on the experimental and theoretical studies but introduce impurity energy levels or induce the formation of OVs/Ti^{3+} defects. Specifically, Irie et al. [83] evaluated the oxidization capability of the $TiO_{2-x}N_x$ powder by the decomposition of gaseous 2-propanol under the same illumination conditions (i.e., the absorbed photon number of visible or UV light was equal to each other). They determined that, regardless of the *x*, the quantum yield from visible light illumination was lower than that from UV light illumination. Moreover, the quantum yield decreased with the increase in the N concentration when irradiated with UV and visible light. Therefore, they concluded that the formation of the isolated and localized midgap state above the VB by N doping (as

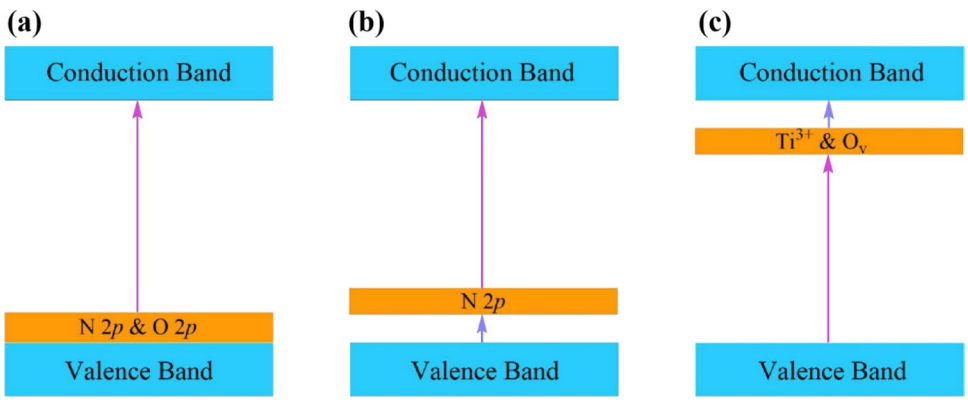

Fig. 5 Three proposed schemes illustrating the possible origin of visible light absorption in N-doped TiO_2: **a** N 2*p* hybridization with O 2*p*, **b** introduction of the localized state above the valence band, and **c** introduction of the localized state below the conduction band. Reproduced from Ref. [100] with permission. Copyright 2010, Royal Society of Chemistry

shown in Fig. 5b) was the cause of the visible light-responsive N-doped TiO_2 materials.

Another point is that the OVs caused by N doping contribute to the absorption and photocatalytic performances in the visible light wavelength range [101], as shown in Fig. 5c. One explanation is that NH_3 can decompose into N_2 and reducing gas H_2 at approximately 550 °C [102]. As a result, the decomposed H_2 can result in the formation of reduced TiO_2 when annealing TiO_2 powder in an NH_3 flow. For instance, Zhao et al. [103] prepared N-doped TiO_2 photocatalysts through a simple solvothermal strategy, followed by a solid-state chemical reduction process. Based on the analysis of the results of the control experiments, they proposed that the reason for the narrowed N–TiO_{2-x} bandgap is the synergetic effect of the defect energy states (including Ti^{3+} and OVs) and N 2*p* midgap state. Another generally accepted explanation is that the OVs are derived from the charge imbalance (N^{3-} vs. O^{2-}) after N doping [90, 104]. Meanwhile, the formation of Ti^{3+} is accompanied by the generation of OVs. This opinion has been verified by Serpone [105], who believe that co-doping N and other anions into the TiO_2 lattice will increase the number of OVs.

Although the aforementioned ideas can explain the reasons for the visible light absorption of N-doped TiO_2 material, there is still no consensus on whether the bandgap can be narrowed and its working mechanism. Therefore, this issue is still open for discussion and in-depth research needs to be conducted.

Characterizations of N-Doped TiO_2 Photocatalysts

The photocatalysis process has been well known to involve three crucial stages, namely, light absorption, charge carriers separation, and surface reaction [106]. Apart from the energy states, which are highly related to the light absorption stage, the investigation of the behavior of photoinduced charge carriers is essential to determine photocatalytic performance. The photoinduced charge carriers are fleetly trapped at the surface states of the photocatalyst particle within sub-picoseconds or a few picoseconds after excitation [107]. Although the lifetime is transitory, the measurement of the transfer kinetic of these charge carriers can provide important information for researchers and reveal the main process in the photocatalytic reaction. Thus far, time-resolved spectroscopy has been proven to be a powerful technique to analyze the charge carriers dynamics of photocatalysts, particularly the photocatalytic processes.

Time-resolved microwave conductivity (TRMC) is one of the powerful technologies employed to investigate the charge carriers dynamics. The obtained TRMC signal decays for TiO_2-based material reflect the change in conductivity caused by the variations of the number of generated electrons. Consequently, the recombination and capture processes of electrons in TiO_2 samples can be determined based on the variations of these signals. Through this technology, Katoh et al. [108] investigated the charge carriers separation and recombination processes in the N-doped TiO_2 photocatalyst. Their results showed that the electronic behavior of N-doped TiO_2 excited by UV light (Ti 3*d* ← O 2*p* transition) was similar to that excited by visible light (450 nm, Ti 3*d* ← N 2*p* transition). However, the trapping rate increased (i.e., the charge carriers separation efficiency of N-doped TiO_2 excited by visible light excitation was one-third of that of pure TiO_2 excited by UV light) in the N-doped sample relative to the undoped sample, which meant that N doping will seriously affect the concentration of OVs.

Yamanaka and Morikawa [109] used femtosecond time-resolved diffuse reflectance (TDR) spectroscopy to elucidate the kinetics of charge carriers separation and trapping in N-doped TiO_2 powder under weak excitation conditions. As shown in Fig. 6a, the TDR spectra of N-doped TiO_2 revealed that the electrons and holes captured on the surface were produced fleetly after excitation, which was similar to that of TiO_2 under 360 nm light excitation (Ti 3*d* ← O 2*p* transition). The additional OVs lead to deep trapping (the time constant is approximately 300 ps); thus, the number of trapped electrons on the surface was lower than that of pure TiO_2. Under 450 nm excitation, the TDR spectra of N-doped TiO_2 showed the signals derived from the Ti 3*d* ← N 2*p* transition. Furthermore, compared with the 360 nm excitation, the 450 nm excitation exhibited two differences in time evolution, i.e., it significantly decreased immediately after excitation and the electron depth was trapped in 1 ps.

In another study, Chen et al. [110] investigated the decay kinetics of photogenerated electrons that result in recombination or carrier reactions in the synthesized N-doped TiO_2 samples using time-resolved infrared (IR) spectroscopy. The observed transient absorbance spectrum at 1910 cm^{-1} shown in Fig. 7a revealed that the $MTiO_2$/Ala-DDA samples exhibited the strongest initial absorption, indicating the existence of a large number of charge carriers. The pure anatase $MTiO_2$/DDA exhibited weaker absorption intensity, indicating that the formation of OVs on tetrahedral Ti^{4+} sites created a shallow donor state below the CB of the $MTiO_2$/Ala-DDA samples. As shown in Fig. 7b, the normalized absorbance decay revealed that the obtained $MTiO_2$/Ala-DDA exhibited a slower decay rate than the two other $MTiO_2$ samples, indicating that the separation of electrons and holes was effectively realized. This may be benefited from the shallow donor state produced by the OVs on tetrahedral Ti^{4+} sites can more effectively promote charge carriers separation and electron capture in $MTiO_2$/Ala-DDA.

Time-resolved absorption (TA) spectroscopy is another powerful and delightful technique to investigate the nature

of photogenerated charge carriers. Tang et al. [111] explored the nature of charge carriers in N-doped films. They explained that the reason for the poor photocatalytic O_2 production from water oxidation of nanocrystalline N-doped TiO_2 film under visible light illumination was mainly the rapid recombination of charge carriers at doping-induced states rather than the deep trapping of photogenerated holes in the bulk material (as shown in Fig. 8). Moreover, they concluded that a long lifetime of no less than 0.4 s for the photogenerated holes was essential to the evolution of O_2 on the nanocrystalline N-doped TiO_2. Therefore, to achieve an improved O_2 evolution efficiency for this doped material, the key strategy is to enhance the charge carriers separation with the aid of cocatalysts, such as Pt cocatalyst.

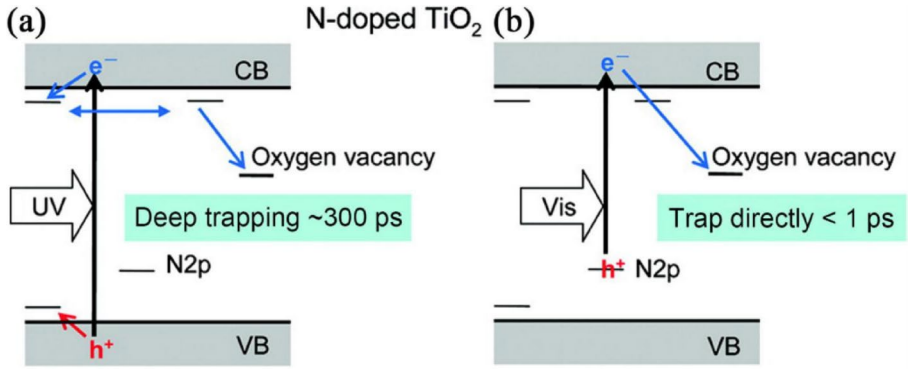

Fig. 6 Schematic diagram of the spatial and energetic distribution of electrons and holes in N-doped TiO_2 powder after excitation under **a** UV light (360 nm) and **b** visible light (450 nm) irradiation. Reproduced from Ref. [109] with permission. Copyright 2010, ACS Publications

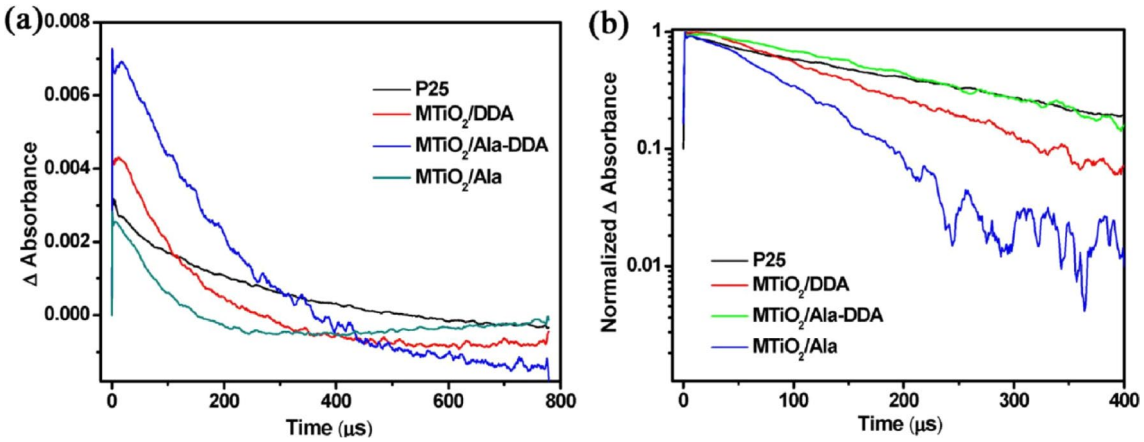

Fig. 7 **a** Temporal profiles of transient infrared absorption in the atmosphere and **b** normalized decay curves at 1910 cm^{-1} of the four catalysts (M: mesoporous, DDA: dodecylamine, Ala: L-alanine acids). Reproduced from Ref. [110] with permission. Copyright 2019

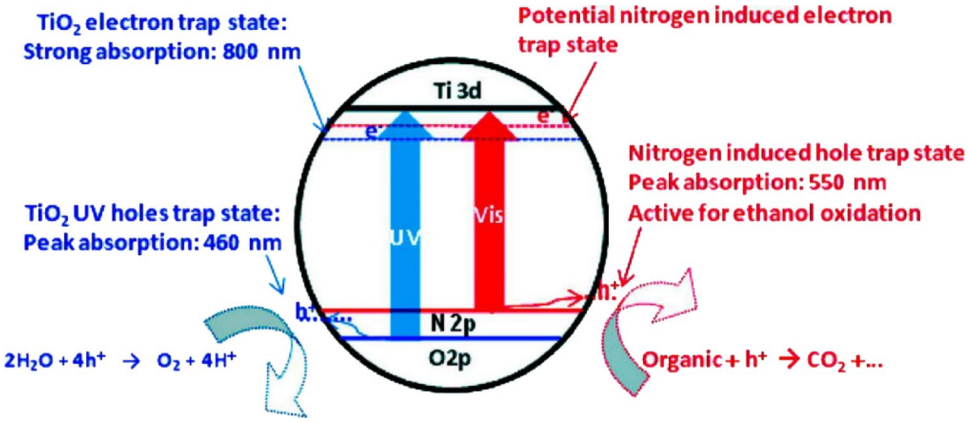

Fig. 8 Band structure of the N-doped TiO_2 sample. Reproduced from Ref. [111] with permission. Copyright 2011, ACS Publications

Main Applications

The aim of engineering functional N-doped TiO_2 samples with well-defined morphologies and crystal phases is to optimize their electronic properties, thereby achieving better performance for photocatalytic applications. In general, a semiconductor-based photocatalytic process usually includes three independent and indispensable steps (Fig. 9) [112], namely, absorption of photons and generation of electron–hole pairs, separation and migration of charge carriers from the matrix to the surface, and surface reactions (i.e., reduction and oxidation reactions). Thus far, tremendous efforts (Table 2) have been exerted to enable the practical applications of N-doped TiO_2 in photooxidation reactions (e.g., photodegradation, photocatalytic disinfection, and O_2 generation from water splitting) or photoreduction reactions (e.g., CO_2 reduction and H_2 generation from water splitting).

Degradation

N-doped TiO_2 material is an effective photocatalytic system for treating some harmful compounds in polluted water/air, and it has been extensively investigated for water treatment and air purification. In the early 2000s, Asahi et al. [58] reported that, under visible light illumination (wavelength < 500 nm), N-doped TiO_2 exhibited better photocatalytic performance for the degradation of methylene blue and gaseous acetaldehyde than undoped TiO_2. Salarian et al. [113] synthesized N-doped TiO_2 via a facile hydrothermal route and investigated the photodegradation performance of diazinon. Their results showed that the degradation and mineralization efficiencies of diazinon could reach 85% and 63%, respectively. Wang et al. [123] showed that N-doped TiO_2 nanoparticles prepared by a post-thermal treatment exhibited enhanced visible light photocatalytic activity for the degradation of methylene blue. Marques et al. [68] used urea as the N source and prepared N-doped TiO_2 nanoparticles with a large specific surface area using the modified sol–gel method. They determined that the doping calcination temperature and molar ratio of urea to TiO_2 have a considerable influence on the N content in N-doped TiO_2 powders. The results of their photocatalytic degradation experiments on methylene blue dye indicated that, under both UV-A light (365 nm) and visible light (400–700 nm) illumination, N-doped TiO_2 exhibited higher photocatalytic efficiency than the pristine TiO_2. Furthermore, the molar ratio of N to TiO_2 used for doping strongly affects the photocatalytic performance of the obtained N-doped TiO_2.

Moreover, the photocatalysis studies on N-doped TiO_2 with different exposed facets revealed different activities. Shi et al. [125] reported that N–TiO_2 plates with dominant facets [001] had superior photocatalytic activities for the degradation of methylene blue under visible light irradiation ($\lambda > 420$ nm) and concluded that the improved performance was attributed to the smaller particle size (approximately 25 nm) and larger specific surface area in comparison with micrometer-sized N-doped TiO_2 materials. Similarly, the [001]-dominated TiO_2 nanosheets co-doped with N and La reported by Wang's group [124] exhibited higher visible light photocatalytic activity for the decomposition of RhB than pure TiO_2, N–TiO_2, La–TiO_2, and N,La–TiO_2 nanoparticles (Fig. 10). This may be because the N, La–TiO_2 nanosheets exhibited the strengthened absorption of visible light than other samples. Moreover, the synergistic effect between N and La, i.e., N doping narrowed the bandgap of TiO_2, whereas La doping improved the separation efficiency of photoelectrons and holes, was attributed to the enhanced photodegradation performance.

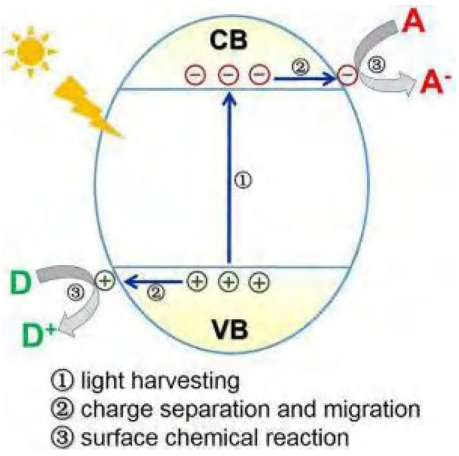

Fig. 9 Schematic illustration of a typical photocatalytic process based on semiconductors. Reproduced from Ref. [112] with permission. Copyright 2019, Elsevier

Sterilization

Photocatalytic disinfection is becoming a promising process for water treatment because it is cost-effective and environmentally safe. Makropoulou et al. [114] used various N precursors (such as urea, TEA, and NH_3) to synthesize N-doped TiO_2 photocatalysts and employed these photocatalysts to inactivate bacteria in an aqueous substrate under simulated sunlight illumination. As shown in Fig. 11, under simulated sunlight illumination, the Gram-negative bacteria *Escherichia coli* and *Pseudomonas aeruginosa* dispersed in solution were successfully inactivated, and the highest reduction rate of 6log10 was reached within 60 min of treatment. In a recent report, Horovitz et al. [115] investigated the efficiency of N-doped TiO_2-coated Al_2O_3 photocatalytic membrane reactors to remove MS2 bacteriophage with different

Table 2 Typical photocatalytic reactions of N-doped TiO_2-based materials

Photocatalyst	Preparation method	UV–Vis absorption	Light source[a]	Application	References
$TiO_{2-x}N_x$ films	Sputtering and calcination	Shoulder absorption	UV light (with a peak at 351 nm) and visible light (with a peak intensity at 436 nm) irradiation	Degradation of methylene blue and acetaldehyde	[58]
N-doped TiO_2	Hydrothermal method	Shoulder absorption	350 W Xe lamp ($380\ nm < \lambda < 900\ nm$)	Degradation of diazinon	[113]
N-doped TiO_2 nanoparticles	Hydrothermal treatment and calcination	Shoulder absorption	LED light (365 nm) and 150 W Xe lamp ($400\ nm < \lambda < 800\ nm$)	Degradation of methylene blue	[68]
N-doped TiO_2	Hydrolysis and calcination	Shoulder absorption	Natural sunlight	Inactivation of *Escherichia coli*, *Pseudomonas aeruginosa*, and *Bacillus cereus*	[114]
N-doped TiO_2 thin film	Sol–gel deposition and calcination	–	300 W solar simulator with a quartz cover placed approximately 6.5 mm above the membrane	Inactivation of MS2	[115]
N-doped TiO_2	Hydrolysis and calcination	Shoulder absorption	Xe lamp ($315\ nm < \lambda < 600\ nm$)	CO_2 reduction	[116]
N-doped anatase TiO_2 microsheets	Hydrothermal method	Shoulder absorption	350 W Xe lamp, UV–Vis and visible light ($\geq 400\ nm$)	CO_2 reduction	[117]
N-doped TiO_2 nanorod arrays	Hydrothermal method	Shoulder absorption	Two 300 W visible light sources (UV < 5%)	CO_2 reduction	[118]
$TiO_{2-x}N_x$	Sol–gel method and calcination	–	Visible light ($\geq 400\ nm$)	O_2 evolution from the oxidation of water	[119]
N-doped TiO_2 nanorods	Sol–gel method and calcination	Shoulder absorption	Visible light ($\geq 400\ nm$)	O_2 evolution from the oxidation of water	[120]
N,F-doped rutile TiO_2	Calcination	Band-to-band absorption	300 W Xe lamp ($420\ nm < \lambda < 800\ nm$), irradiated through a water filter	Z-scheme water splitting for O_2/H_2 evolution[b]	[94]
B,N-doped TiO_2	Hydrothermal method and calcination	Band-to-band absorption	300 W Xe lamp ($\geq 420\ nm$)	Water splitting for O_2/H_2 evolution	[96]
C,N-doped TiO_2	Aqueous precipitation reaction and calcination	Band-to-band absorption	300 W Xe lamp ($\geq 420\ nm$)	O_2 evolution from the oxidation of water	[97]
N-doped TiO_2	Hydrolysis and calcination	Shoulder absorption	300 W Xe lamp ($\geq 400\ nm$)	H_2 evolution from the reduction of water	[121]
N-doped TiO_2 nanobelts	Hydrothermal method and calcination	Shoulder absorption	300 W Xe lamp ($400\ nm < \lambda < 800\ nm$)	H_2 evolution from the reduction of water	[122]

[a]Xe lamp: xenon lamp.

[b]Z-scheme water splitting was conducted with $Ru/SrTiO_3$:Rh (25 mg) and RuO_2/TiO_2:N,F (50 mg) catalysts in an aqueous tris(2,2′-bipyridyl) cobalt(II) sulfate ($[Co(bpy)_3]^{2+}$, 0.5 mmol/L) solution (120 mL)

water qualities. Their results showed that the hybrid reactors exhibited high efficiency in inactivating the MS2 virus.

Organic Transformation

Photocatalytic organic transformation as a green, sustainable, and environmentally friendly technique has received increasing attention, and many organic materials with special functions were synthesized via selective oxidation or reduction with the aid of photocatalysts in recent years. For instance, Japa et al. [126] investigated the selective transformation of benzyl alcohol and benzylamine into benzaldehyde and benzylamine under visible light illumination using N-doped TiO_2 as catalysts, which were prepared by thermal hydrolysis of $TiOSO_4$ using NH_4OH as both precipitating agent and N source. As shown in Fig. 12, the

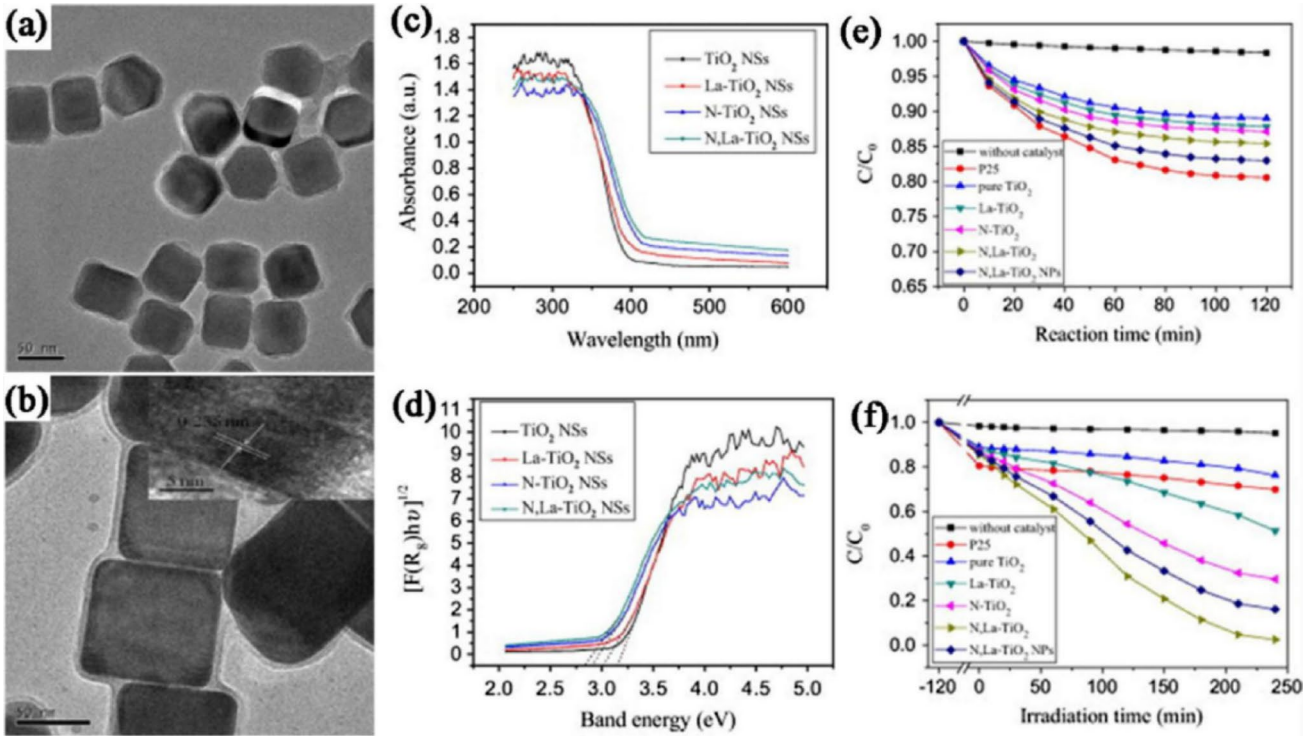

Fig. 10 **a, b** TEM of N,La–TiO_2 nanosheets; **c** UV–Vis diffuse reflectance spectrum and **d** plots of $[F(R\infty)h\nu]^{1/2}$ vs. photon energy of the samples of TiO_2, La–TiO_2, N–TiO_2, and N,La–TiO_2 nanosheets; **e** adsorption of RhB (10 mg/L) in the dark; and **f** degradation of RhB with different photocatalysts under visible light irradiation. Reproduced from Ref. [124] with permission. Copyright 2015, Elsevier

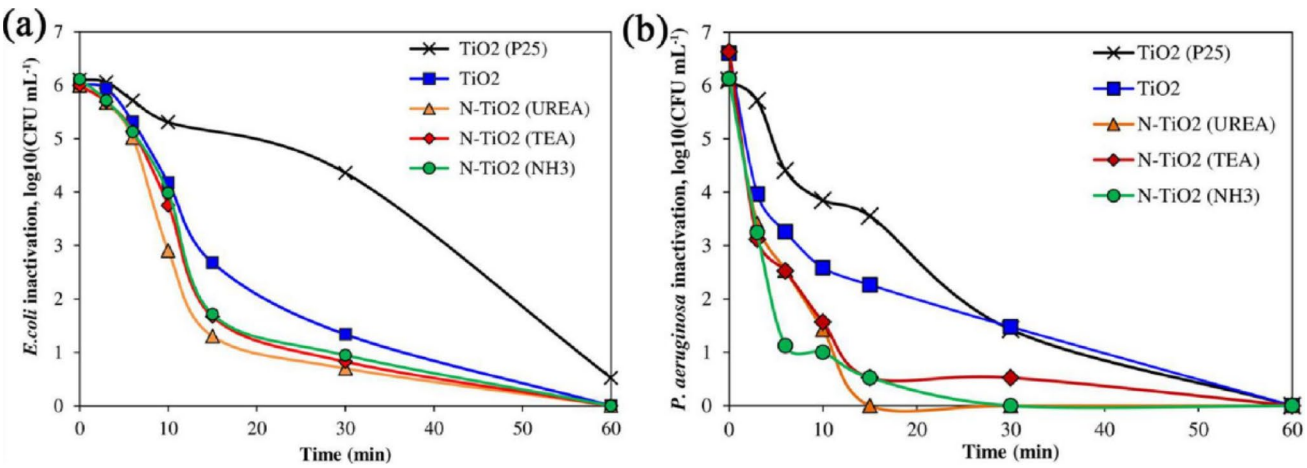

Fig. 11 Inactivation of **a** *Escherichia coli* and **b** *Pseudomonas aeruginosa* under simulated sunlight illumination in the presence of N-doped TiO_2 photocatalysts (fabricated using different N precursors), pristine TiO_2, and P25 TiO_2. Reproduced from Ref. [114] with permission. Copyright 2018, Wiley–VCH

optimized N-doped TiO_2 (T_400) exhibited superior photocatalytic activity for the selective oxidation of benzyl alcohol and benzylamine to benzaldehyde and N-benzylidenebenzylamine products, respectively, with > 85% conversion and > 95% selectivity, regardless of the substituents of the benzylamine molecule. The control sample (T_400_NaOH), prepared using NaOH (instead of NH_4OH) as precipitating agent, was also analyzed, and the results revealed the beneficial nature of N doping for selective oxidation.

Singha et al. [67] synthesized N-doped yellow TiO_2 hollow spheres using aqueous titanium peroxocarbonate complex solution as a precursor and NH_4OH and used them to

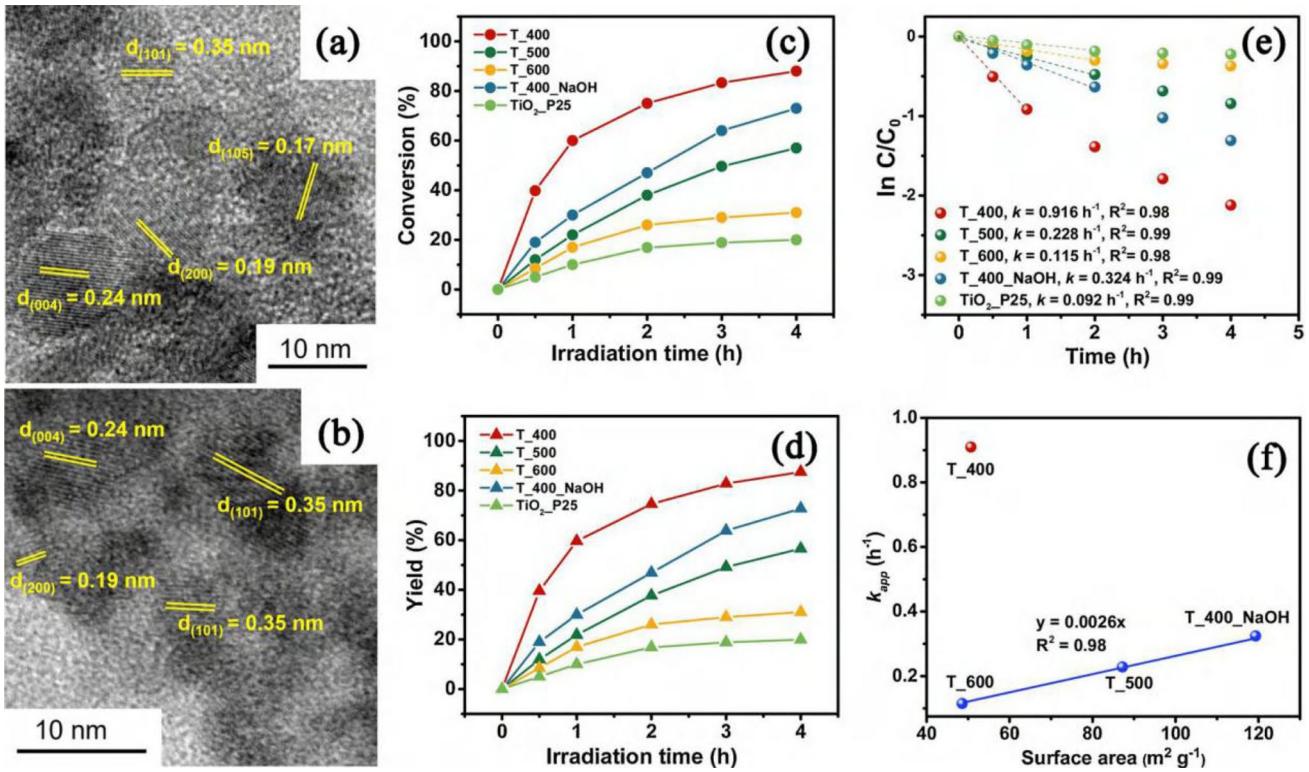

Fig. 12 HRTEM of **a** T_400 and **b** T_400_NaOH; **c** photocatalytic conversion of benzyl alcohol; **d** evolution of the benzaldehyde product; **e** corresponding initial pseudo-first-order kinetics of different catalysts at an optical power of approximately 75 mW/cm^2; and **f** relationship between apparent pseudo-first-order rate constant and catalyst surface area. Reproduced from Ref. [126] with permission. Copyright 2021, Elsevier

promote the synthesis of active esters of N-hydroxyimide and alcohol through simultaneous selective oxidation of alcohol to aldehyde, followed by cross-dehydrogenative coupling via visible light illumination under ambient conditions. Xu et al. [127] fabricated N-doped anatase/rutile mixed-phase TiO_2 photocatalysts with carbonaceous species by pyrolyzing MIL-125 (Ti) and P25 composites as the precursor and subsequently doping N into the pyrolysis product using urea as the dopant. In this study, the photocatalysts showed excellent performances of photocatalytic cyclohexane oxidation under visible light illumination. The yield of KA oil (cyclohexanol and cyclohexanone) reached 112.44 μmol after 5-h illumination of the photocatalyst with the optimal N-doped anatase/rutile ratio, which was 5.66 and 39.87 times that of N-doped anatase TiO_2 and N-doped P25, respectively. In the meantime, the selectivity toward cyclohexanone could reach 100%. Cipagauta-Díaz's group [128] tested the photocatalytic activity of N-doped TiO_2 materials, which were synthesized by a low-temperature microwave-assisted sol–gel method, in the photoreduction of 4-nitrophenol (4-NP) to 4-aminophenol under a visible light source. Although the enhanced photoreduction of 4-NP for N-doped TiO_2 (TiEN*0.5 and TiEN*1) in comparison with bare TiO_2 was obtained (Fig. 13), the utilization of visible light has a low efficiency.

CO_2 Reduction

The photocatalytic reduction of CO_2 to hydrocarbons has considerable potential to provide alternative fuel to the world and solve the CO_2 emission problem. Since the first report by Inoue et al. [129], tremendous efforts have been exerted to enhance the efficiency of TiO_2-based catalysts for photocatalytic CO_2 reduction. For instance, Bjelajac et al. [116] synthesized N-doped TiO_2 nanoparticles and investigated their photocatalytic CO_2 reduction performance. The results shown in Fig. 14 indicated that the N-doped sample exhibited superior production rates of H_2, CH_4, and CO. By contrast, the P25 catalyst did not affect the productivity of CH_4. One reason for this phenomenon is that the bandgap of the obtained N-doped TiO_2 is smaller; thus, the photon absorption is higher than that of P25. The other reason is the optimal grain sizes of the synthetic samples, as the particles of the P25 sample are generally larger. The larger the grain size is, the lower the charge carriers separation, thus leading to a higher electron consumption rate.

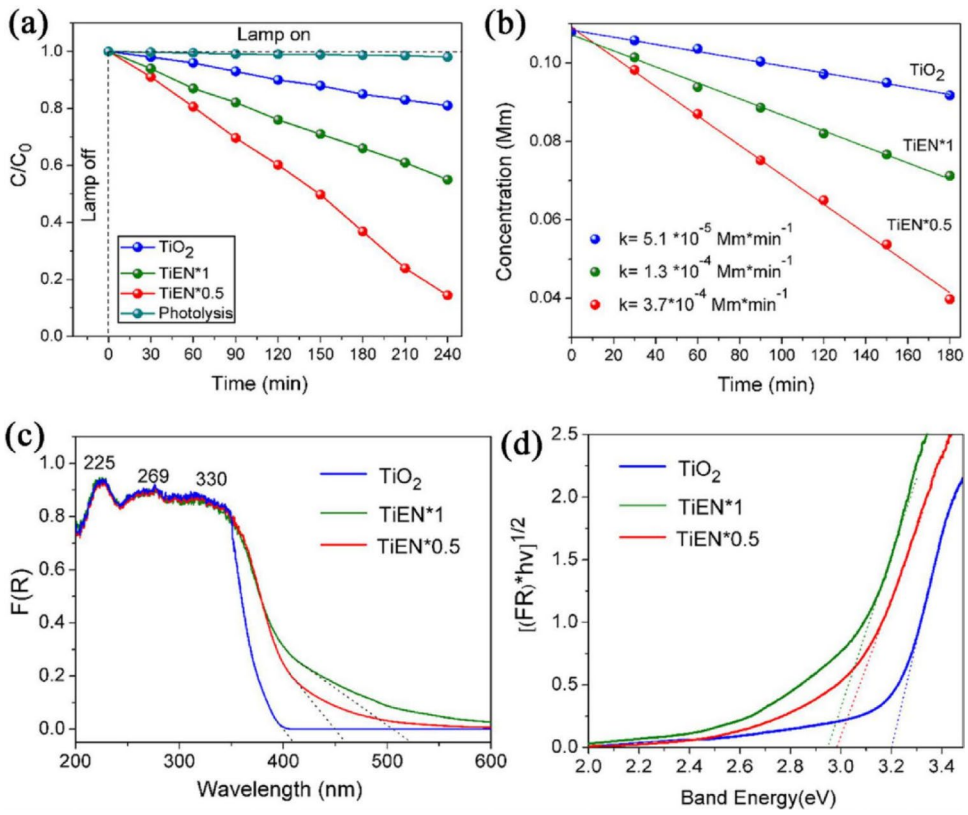

Fig. 13 **a** C/C_0 plot as a function of time for 4-nitrophenol (4-NP) photoreduction; **b** zero-order kinetics plot of 4-NP photoreduction; **c** diffuse reflectance spectroscopy UV–Vis spectra; and **d** Kubelka–Munk modified spectra of the materials TiO_2, TiEN*0.5, and TiEN*1. Reproduced from Ref. [128] with permission. Copyright 2020, Wiley–VCH

To improve the separation efficiency of photoinduced charge carriers, Akple et al. [117] prepared visible light-responsive N-doped anatase TiO_2 microsheets, which have a heterojunction structure with 65% (101) and 35% (001) exposed faces, through a hydrothermal route. Under visible light irradiation, the obtained N-doped TiO_2 exhibited better photocatalytic performance for CO_2 reduction than pure TiN and P25 because of the synergistic effect of surface heterojunctions to improve electron–hole separation and N doping, which is beneficial to visible light absorption. Apart from the pretreatments and surface heterojunctions, the selection of N sources also has an effect on the photocatalytic activity of the N-doped TiO_2 catalyst. Zhang et al. [118] demonstrated that the N–N group in the N source (N_2H_4 or NH_3) plays a decisive role in the selectivity of the main product of photocatalytic reduction on the surface of the obtained N-doped TiO_2 catalysts. They determined that, under visible light illumination, the main products of N–TiO_2 doped with N_2H_4 and NH_3 were CH_4 and CO, respectively. Therefore, they concluded that the presence of N–N groups on the surface of N_2H_4-doped N–TiO_2 provided a reducing environment, which caused CH_4 to become the main reduction product.

Water Splitting

From the perspective of converting solar energy into fuel energy, photocatalytic water splitting has attracted considerable attention. In terms of N-doped TiO_2, scientists have exerted tremendous efforts to investigate the mechanisms and properties under visible light illumination. Yun et al. [119] evaluated the effects of the amount of N in N-doped TiO_2 nanoparticles on O_2 generation via visible light-driven water oxidation and claimed that a small amount of N dopant (up to 3 at%) added to the samples can accelerate the production of O_2 instead of the formation of $OH^{\bullet}$ species. However, larger amounts of N dopant doped into $TiO_{2-x}N_x$ can reduce the rates of both O_2 production and $OH^{\bullet}$ formation, which can be attributed to the low energy level of the VB and the short lifetime of the photoinduced charge carriers. Lee et al. [120] described the improvement of O_2 evolution from water oxidation on the N-doped TiO_2 nanospheres and nanorods prepared by calcination in NH_3 flow. The measurement of photocatalytic activities showed that the two N-doped samples exhibited enhanced O_2 evolution performance than the undoped samples. Recently, Liu's group [96] developed a new nitrogenation method to dope uniform B and N into

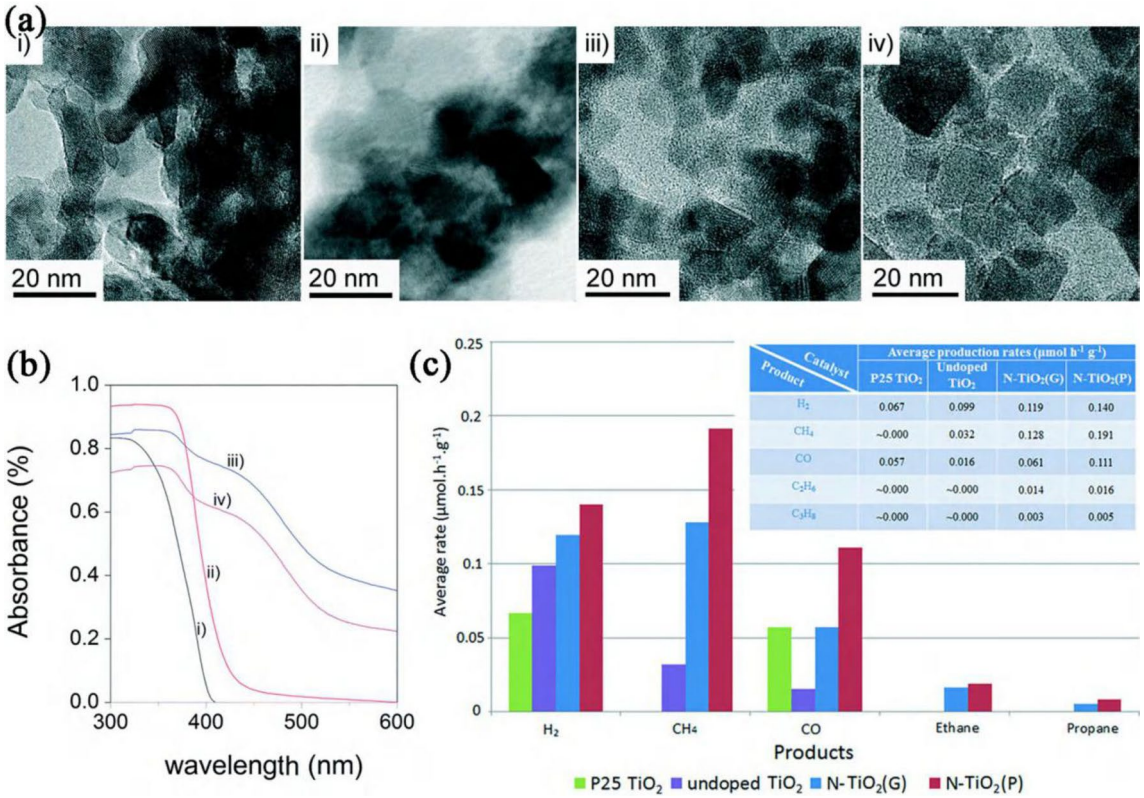

Product \ Catalyst	P25 TiO_2	Undoped TiO_2	N-TiO_2(G)	N-TiO_2(P)
	Average production rates (μmol h^{-1} g^{-1})			
H_2	0.067	0.099	0.119	0.140
CH_4	~0.000	0.032	0.128	0.191
CO	0.057	0.016	0.061	0.111
C_2H_6	~0.000	~0.000	0.014	0.016
C_3H_8	~0.000	~0.000	0.003	0.005

Fig. 14 **a** TEM micrographs and **b** absorption spectra of the investigated samples: (i) P25 TiO_2, (ii) undoped TiO_2, (iii) N–TiO_2(G), and iv) N–TiO_2(P). **c** Average yield rates of each product for all catalysts ("G" denotes that the gel was directly annealed in an NH_3 atmosphere in a tube furnace, whereas "P" denotes that the gel was pre-annealed in air at 500 °C for 3 h and annealed in an NH_3 atmosphere). Reproduced from Ref. [116] with permission. Copyright 2020, Royal Society of Chemistry

TiO_2 microspheres with exposed facets [001], as shown in Fig. 15a–e. The obtained red TiO_2 did not show an increase in defects (such as Ti^{3+}), which usually exist in doped TiO_2. This decrement may be the result of charge compensation between interstitial B^{3+} and substituted N^{3-}, which can hinder the formation of new OVs in the uniform B,N-co-doped TiO_2. After loading the RuO_2 cocatalyst, the red TiO_2 exhibited a higher photocatalytic O_2 evolution activity and stability than the pristine TiO_2 (Fig. 15f, g). In their work, Wu et al. [97] reported that a C, N substitute was uniformly doped into anatase TiO_2 decahedral plates. Because of the uniform C,N co-doping to narrow the bandgap, the obtained $TiO_{2-x}(CN)_y$ sample had an ideal spectrum of strong band-to-band visible light absorption, which had the capability to induce water oxidation to generate O_2 with CoO_x that used as cocatalyst under visible light illumination.

In addition to photocatalytic O_2 evolution, N-doped TiO_2 materials are often used as photocatalysts for H_2 generation from water reduction. Shangguan and co-workers [121] prepared N-doped TiO_2 catalysts with large specific surface areas by calcining a mixture of TiO_2 and urea and investigated their photocatalytic H_2 generation activity. They confirmed the existence of N on TiO_2 as chemisorbed N_2 molecules and substitutional N on TiO_2 via XPS measurements and summarized that the crystalline phase of TiO_2 and the substitutional N were the main factors improving the photocatalytic performance of water reduction for H_2 generation. Sun et al. [122] prepared anatase N-doped TiO_2 nanobelts with a surface heterojunction of co-exposed facets (101) and (001) and measured their photocatalytic water splitting performance. Based on the research findings, they proposed that, during the catalytic process, the surface heterojunction not only promoted the disintegration of water molecules but also enhanced the space separation of charge carriers to effectively inhibit the recombination of the charge carriers (Fig. 16), thus achieving water reduction for H_2 production under visible light stimulation. The B,N-co-doped TiO_2 prepared by Liu et al. [97] also had the photocatalytic capability to convert water into H_2 when loaded with 0.5 wt% Pt cocatalyst and methanol utilized as a sacrificial agent under visible light illumination.

Although the investigation of N,F-co-doped anatase TiO_2 has been reported, only a few reports are available for the rutile form. In recent work, Maeda et al. [94] focused on N,F-co-doped rutile TiO_2 material (R-TiO_2:N,F), which was synthesized via a nitridation process at 500 °C using

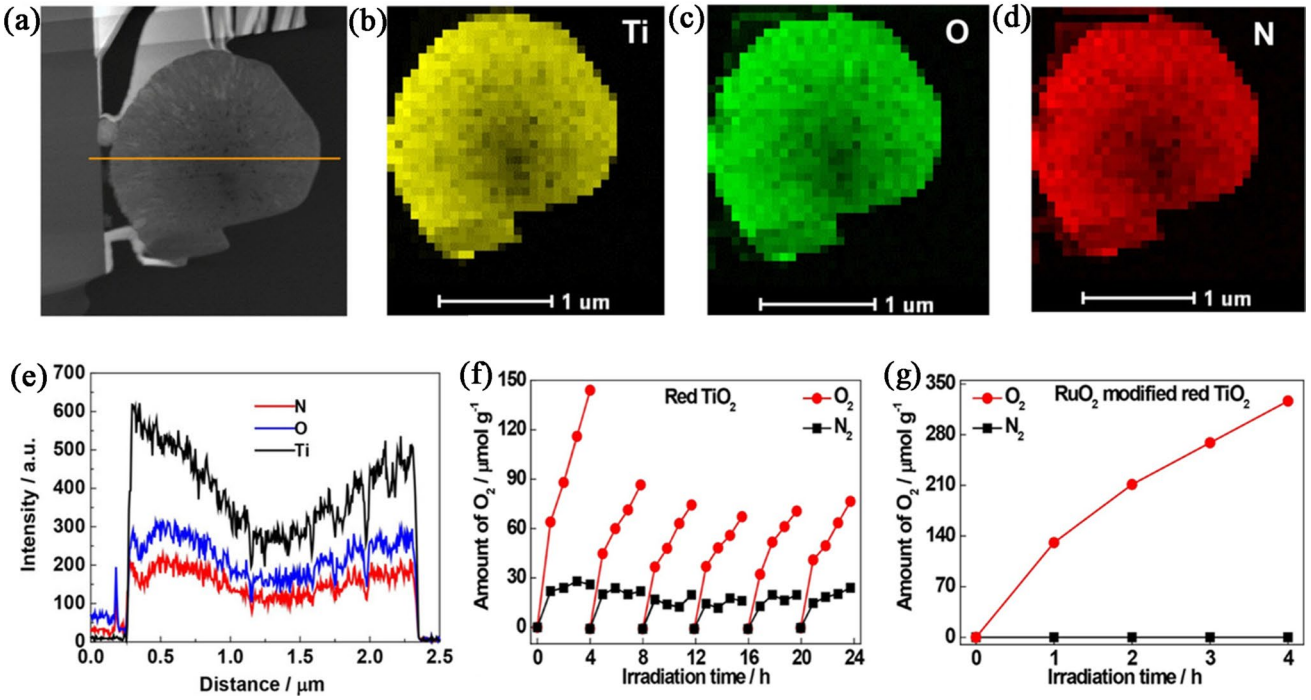

Fig. 15 **a** Scanning TEM high-angle annular dark field image and **b**–**d** EDS elemental mapping images of Ti–K, O–K, and N–K recorded from the sheet shown in **a**. **e** Line-scan profiles of Ti–K, O–K, and N–K along the orange line in **a**. **f** Cycling tests of the photocatalytic production of O_2 from an $AgNO_3$ aqueous solution through B, N-doped TiO_2 microspheres as a function of the exposure time to visible light. **g** Photocatalytic O_2 evolution from an $AgNO_3$ aqueous solution through B, N-doped TiO_2 modified with 1 wt% RuO_2 cocatalyst as a function of the exposure time to visible light. Reproduced from Ref. [96] with permission. Copyright 2019, Wiley–VCH

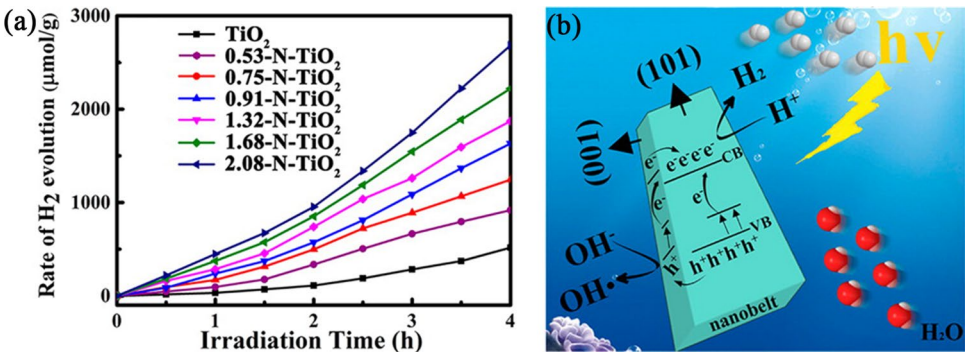

Fig. 16 **a** H_2 production rates and **b** diagram of the charge shift process in N-doped TiO_2 nanobelts. Reproduced from Ref. [122] with permission. Copyright 2016, American Chemical Society

rutile TiO_2 and $(NH_4)_2TiF_6$ as raw materials, as O_2 generation photocatalyst for visible light-driven Z-scheme water splitting (Fig. 17a–d). Notably, the prepared samples showed clear absorption in the visible region, and the more pronounced visible light absorption in the present R-TiO_2:N,F samples was attributed to the increased N content. This material exhibited water oxidation activity with the help of the RuO_2 cocatalyst even in the presence of a reversible electron acceptor, such as IO_3^- or Fe^{3+}. However, water reduction activity was not observed because of the high Ti^{3+} concentration, which was evidenced by the absorption at longer wavelengths ($\lambda > 600$ nm) [130]. By contrast, as shown in Fig. 17g, the combination of RuO_2-loaded R-TiO_2:N,F and Ru/$SrTiO_3$:Rh photocatalysts could be used as a visible light-driven Z-scheme water splitting system with $[Co(bpy)_3]^{3+/2+}$ acts as a shuttle redox mediator and exhibited a stoichiometric photocatalytic overall water splitting activity with long-term stability.

Although the solar energy conversion efficiencies of these materials are still low, the methodologies proposed in these studies should contribute to the improvement of the photocatalytic performance of N-doped TiO_2-based visible light-responsive materials.

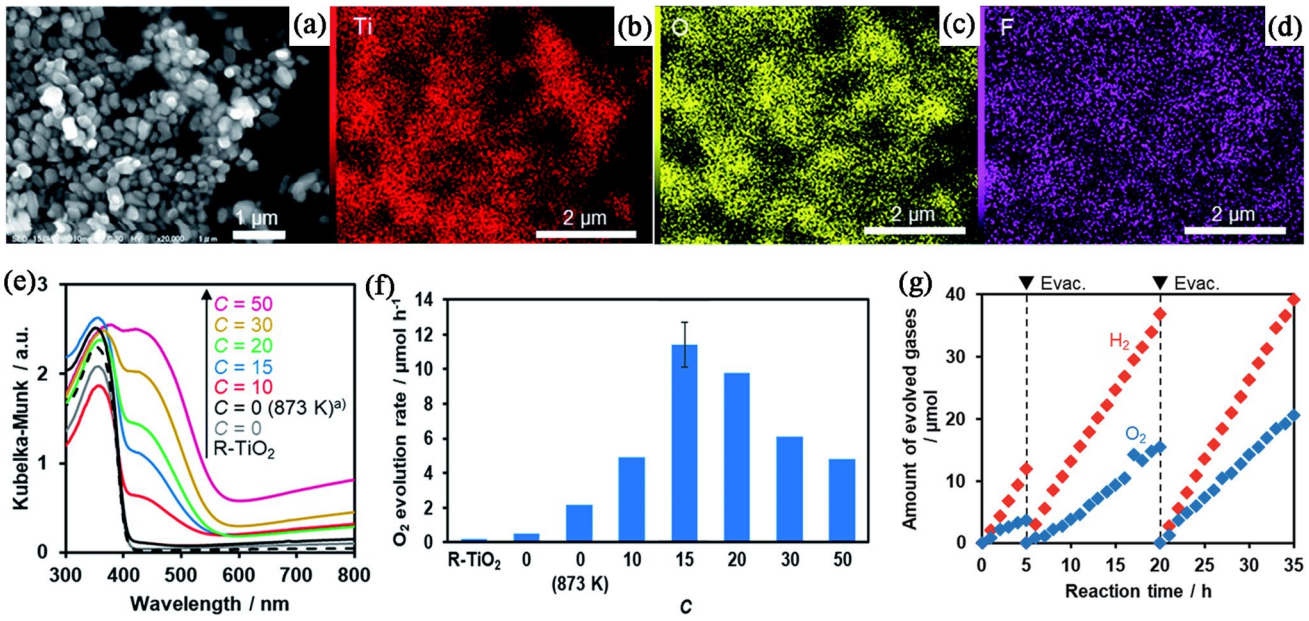

Fig. 17 **a** SEM image, **b–d** EDX elemental mapping data, and **e** UV–Vis diffuse reflectance spectra of R-TiO_2:N,F. **f** Photocatalytic activity of R-TiO_2:N,F for O_2 evolution under visible light irradiation in $AgNO_3$ aqueous solution. Reaction conditions: catalyst, 50 mg; La_2O_3, 200 mg; 10 mmol/LL $AgNO_3$ aqueous solution, 140 mL; light source, 300 W Xe lamp fitted with a 420-nm cutoff filter. **g** Time course of H_2 and O_2 evolution from mixtures of RuO_2/R-TiO_2:N,F (50 mg) and Ru/$SrTiO_3$:Rh (25 mg) dispersed in an aqueous solution (120 mL) containing tris(2,20-bipyridyl)cobalt(II) sulfate (0.5 mmol/LL) under visible light irradiation ($\lambda > 420$ nm). Reproduced from Ref. [94] with permission. Copyright 2018, Royal Society of Chemistry

Summary and Outlook

This review attempts to provide a comprehensive update and summary focusing on the synthesis, characterizations, and practical applications of visible light-responsive N-doped TiO_2 photocatalyst. N-doped TiO_2 not only effectively reduces the bandgap but also reduces the recombination efficiency of photoinduced charge carriers. Although the detailed source of photocatalysis of this material remains a debate, its basic principles and mechanisms have guided the search for other novel similar photocatalysis materials. Generally, the photocatalytic reaction rates of N-doped TiO_2 are still low. The findings can be attributed to the fact that the visible light absorption of N-doped samples is still poor, which cannot achieve the ideal band-to-band absorption. Moreover, with the increase in N content, the introduced OVs can act as recombination centers, thus resulting in a decreased photocatalytic reaction rate. Despite tremendous efforts that have been exerted in the area of enhancing the visible light absorption of TiO_2-based materials, the following investigations need to be conducted in the future:

(1) To explore the synergistic effect of various synthesis strategies, as no single solution can make materials suitable for different applications;

(2) How co-doping of various N precursors and other nonmetals affects the band structure and photocatalytic performance of TiO_2 remains to be clarified;

(3) Although most of these N-doped TiO_2 samples can individually produce H_2 or O_2 from H_2O splitting in the presence of appropriate sacrificial agents under visible light illumination, which indicates that overall water splitting is possible in principle, it has not yet been realized. Further effort is required to realize the utilization of TiO_2-based catalysts in photocatalytic overall water splitting activity under visible light irradiation;

(4) The use of cocatalysts in photocatalytic water splitting systems can not only provide more active sites for redox reactions on the surface of the semiconductors but also accelerate the extraction and transfer of generated electrons for surface reactions. Recently, single-atom catalysts (SACs) with 100% atom utilization have shown superior performances in heterogeneous catalysis fields, such as photocatalytic reactions. In a sense, SACs could be employed as cocatalysts for N-doped TiO_2 materials to enhance their photocatalytic activities because of their fascinating strengths in enhancing light harvesting, charge transfer dynamics, and surface reactions of a photocatalytic system;

(5) Conjugated polymers (CPs) have been used to produce solar energy conversion materials in photovoltaics because of their outstanding light-harvesting and low-

cost processing. However, their photocatalytic activity has only recently been highlighted with the preparation of robust, metal-free, and visible or near-IR light-active photocatalysts. In the future, hybrid photocatalysts based on N-doped TiO_2 semiconductors and CPs can be fabricated and used as novel promising photoactive materials for pollutant degradation, energy conversion through water splitting, and/or CO_2 reduction using photocatalytic processes.

Acknowledgements This work was supported by the National Natural Science Foundation of China (Nos. 21633009, 21925206, 21901240) and the National Key Research and Development Program of China (No. 2020YFA0406102).

Declarations

Conflict of interest The authors declare that there is no conflict of interest.

References

1. Fujishima A, Honda K (1972) Electrochemical photolysis of water at a semiconductor electrode. Nature 238(5358):37–38
2. Fujishima A, Rao T, Tryk DA (2000) Titanium dioxide photocatalysis. J Photochem Photobiol C Photochem Rev 1(1):1–21
3. Ahmad H, Kamarudin SK, Minggu LJ et al (2015) Hydrogen from photo-catalytic water splitting process: a review. Renew Sustain Energy Rev 43:599–610
4. Zhang JL, Tian BZ, Wang LZ et al (2018) Photocatalysis. Springer, Singapore
5. Ge MZ, Cao CY, Huang JY et al (2016) A review of one-dimensional TiO_2 nanostructured materials for environmental and energy applications. J Mater Chem A 4(18):6772–6801
6. Yamakata A, Vequizo JJM (2019) Curious behaviors of photogenerated electrons and holes at the defects on anatase, rutile, and brookite TiO_2 powders: a review. J Photochem Photobiol C Photochem Rev 40:234–243
7. Liu LJ, Zhao HL, Andino JM et al (2012) Photocatalytic CO_2 reduction with H_2O on TiO_2 nanocrystals: comparison of anatase, rutile, and brookite polymorphs and exploration of surface chemistry. ACS Catal 2(8):1817–1828
8. Diebold U (2003) The surface science of titanium dioxide. Surf Sci Rep 48(5–8):53–229
9. Zhang JF, Zhou P, Liu JJ et al (2014) New understanding of the difference of photocatalytic activity among anatase, rutile and brookite TiO_2. Phys Chem Chem Phys 16(38):20382–20386
10. Zhang JF, Wageh S, Al-Ghamdi A et al (2016) New understanding on the different photocatalytic activity of wurtzite and zinc-blende CdS. Appl Catal B Environ 192:101–107
11. Wu W, Jiang C, Roy VA (2015) Recent progress in magnetic iron oxide-semiconductor composite nanomaterials as promising photocatalysts. Nanoscale 7(1):38–58
12. Yang YQ, Yin LC, Gong Y et al (2018) An unusual strong visible-light absorption band in red anatase TiO_2 photocatalyst induced by atomic hydrogen-occupied oxygen vacancies. Adv Mater 30(6):1704479
13. Hu Z, Li KN, Wu XF et al (2019) Dramatic promotion of visible-light photoreactivity of TiO_2 hollow microspheres towards NO oxidation by introduction of oxygen vacancy. Appl Catal B Environ 256:117860
14. Wang Z, Lang XJ (2018) Visible light photocatalysis of dye-sensitized TiO_2: the selective aerobic oxidation of amines to imines. Appl Catal B Environ 224:404–409
15. Lang XJ, Zhao JC, Chen XD (2016) Visible-light-induced photoredox catalysis of dye-sensitized titanium dioxide: selective aerobic oxidation of organic sulfides. Angew Chem Int Ed 55(15):4697–4700
16. Dahlman C, Agrawal A, Staller CM et al (2019) Anisotropic origins of localized surface plasmon resonance in n-type anatase TiO_2 nanocrystals. Chem Mater 31(2):502–511
17. Gao YY, Nie W, Zhu QH et al (2020) The polarization effect in surface-plasmon-induced photocatalysis on Au/TiO_2 nanoparticles. Angew Chem Int Ed 59(41):18218–18223
18. George S, Pokhrel S, Ji ZX et al (2011) Role of Fe doping in tuning the band gap of TiO_2 for the photo-oxidation-induced cytotoxicity paradigm. J Am Chem Soc 133(29):11270–11278
19. Biswas A, Chakraborty A, Jana NR (2018) Nitrogen and fluorine codoped, colloidal TiO_2 nanoparticle: tunable doping, large red-shifted band edge, visible light induced photocatalysis, and cell death. ACS Appl Mater Interfaces 10(2):1976–1986
20. Kapilashrami MY, Liu YS et al (2014) Probing the optical property and electronic structure of TiO_2 nanomaterials for renewable energy applications. Chem Rev 114(19):9662–9707
21. Ismael M (2020) Enhanced photocatalytic hydrogen production and degradation of organic pollutants from Fe (III) doped TiO_2 nanoparticles. J Environ Chem Eng 8(2):103676
22. Sadanandam G, Lalitha K, Kumari VD et al (2013) Cobalt doped TiO_2: a stable and efficient photocatalyst for continuous hydrogen production from glycerol: water mixtures under solar light irradiation. Int J Hydrog Energy 38(23):9655–9664
23. Li XH, Wu Y, Shen YH et al (2018) A novel bifunctional Ni-doped TiO_2 inverse opal with enhanced SERS performance and excellent photocatalytic activity. Appl Surf Sci 427:739–744
24. Camarillo R, Rizaldos D, Jiménez C et al (2019) Enhancing the photocatalytic reduction of CO_2 with undoped and Cu-doped TiO_2 nanofibers synthesized in supercritical medium. J Supercrit Fluids 147:70–80
25. Pérez-Larios A, Hernández-Gordillo A, Morales-Mendoza G et al (2016) Enhancing the H_2 evolution from water-methanol solution using Mn^{2+}–Mn^{+3}–Mn^{4+} redox species of Mn-doped TiO_2 sol-gel photocatalysts. Catal Today 266:9–16
26. Feng SJ, Zhao J, Bai YJ et al (2020) Facile synthesis of Mo-doped TiO_2 for selective photocatalytic CO_2 reduction to methane: promoted H_2O dissociation by Mo doping. J CO2 Util 38:1–9
27. Li YY, Walsh AG, Li DS et al (2020) W-doped TiO_2 for photothermocatalytic CO_2 reduction. Nanoscale 12(33):17245–17252
28. Wang HY, Chen JZ, Xiao FX et al (2016) Doping-induced structural evolution from rutile to anatase: formation of Nb-doped

anatase TiO_2 nanosheets with high photocatalytic activity. J Mater Chem A 4(18):6926–6932
29. Kočí K, Troppová I, Reli M et al (2018) Nd/TiO_2 anatase-brookite photocatalysts for photocatalytic decomposition of methanol. Front Chem 6:44
30. Huang CY, Guo RT, Pan WG et al (2018) Eu-doped TiO_2 nanoparticles with enhanced activity for CO_2 phpotcatalytic reduction. J CO2 Util 26:487–495
31. Singh K, Harish S, Kristy AP et al (2018) Erbium doped TiO_2 interconnected mesoporous spheres as an efficient visible light catalyst for photocatalytic applications. Appl Surf Sci 449:755–763
32. Peng H, Guo RT, Lin H (2020) Photocatalytic reduction of CO_2 over Sm-doped TiO_2 nanoparticles. J Rare Earths 38(12):1297–1304
33. Ribao P, Corredor J, Rivero MJ et al (2019) Role of reactive oxygen species on the activity of noble metal-doped TiO_2 photocatalysts. J Hazard Mater 372:45–51
34. Zhang YY, Hu HW, Chang ML et al (2017) Non-uniform doping outperforms uniform doping for enhancing the photocatalytic efficiency of Au-doped TiO_2 nanotubes in organic dye degradation. Ceram Int 43(12):9053–9059
35. Ida S, Sato K, Nagata T et al (2018) A cocatalyst that stabilizes a hydride intermediate during photocatalytic hydrogen evolution over a rhodium-doped TiO_2 nanosheet. Angew Chem Int Ed Engl 57(29):9073–9077
36. Bilgin SE (2017) Solvothermal synthesized boron doped TiO_2 catalysts: photocatalytic degradation of endocrine disrupting compounds and pharmaceuticals under visible light irradiation. Appl Catal B Environ 200:309–322
37. Wang WK, Chen JJ, Gao M et al (2016) Photocatalytic degradation of atrazine by boron-doped TiO_2 with a tunable rutile/anatase ratio. Appl Catal B Environ 195:69–76
38. Shao J, Sheng WC, Wang MS et al (2017) In situ synthesis of carbon-doped TiO_2 single-crystal nanorods with a remarkably photocatalytic efficiency. Appl Catal B Environ 209:311–319
39. Jia GR, Wang Y, Cui XQ et al (2018) Highly carbon-doped TiO_2 derived from MXene boosting the photocatalytic hydrogen evolution. ACS Sustain Chem Eng 6(10):13480–13486
40. Wang J, de Tafen N, Lewis JP et al (2009) Origin of photocatalytic activity of nitrogen-doped TiO_2 nanobelts. J Am Chem Soc 131(34):12290–12297
41. Boningari T, Inturi SNR, Suidan M et al (2018) Novel one-step synthesis of nitrogen-doped TiO_2 by flame aerosol technique for visible-light photocatalysis: effect of synthesis parameters and secondary nitrogen (N) source. Chem Eng J 350:324–334
42. Gao QZ, Si FY, Zhang SS et al (2019) Hydrogenated F-doped TiO_2 for photocatalytic hydrogen evolution and pollutant degradation. Int J Hydrog Energy 44(16):8011–8019
43. Xie RJ, Lei DX, Zhan YJ et al (2020) Efficient photocatalytic oxidation of gaseous toluene over F-doped TiO_2 in a wet scrubbing process. Chem Eng J 386:121025
44. Boningari T, Inturi SNR, Suidan M et al (2018) Novel one-step synthesis of sulfur doped-TiO_2 by flame spray pyrolysis for visible light photocatalytic degradation of acetaldehyde. Chem Eng J 339:249–258
45. Yuan W, Cheng L, An Y et al (2018) Laminated hybrid junction of sulfur-doped TiO_2 and a carbon substrate derived from Ti_3C_2 MXenes: toward highly visible light-driven photocatalytic hydrogen evolution. Adv Sci (Weinh) 5(6):1700870
46. Xu H, Zheng Z, Zhang L et al (2008) Hierarchical chlorine-doped rutile TiO_2 spherical clusters of nanorods: large-scale synthesis and high photocatalytic activity. J Solid State Chem 181(9):2516–2522
47. Wang XK, Wang C, Jiang WQ et al (2012) Sonochemical synthesis and characterization of Cl-doped TiO_2 and its application in the photodegradation of phthalate ester under visible light irradiation. Chem Eng J 189–190:288–294
48. Lin HY, Shih CY (2016) Efficient one-pot microwave-assisted hydrothermal synthesis of M (M = Cr, Ni, Cu, Nb) and nitrogen co-doped TiO_2 for hydrogen production by photocatalytic water splitting. J Mol Catal A Chem 411:128–137
49. Kumar MK, Bhavani K, Srinivas B et al (2016) Nano structured bismuth and nitrogen co-doped TiO_2 as an efficient light harvesting photocatalyst under natural sunlight for the production of H_2 by H_2O splitting. Appl Catal A Gen 515:91–100
50. Kim TH, Rodríguez-González V, Gyawali G et al (2013) Synthesis of solar light responsive Fe, N co-doped TiO_2 photocatalyst by sonochemical method. Catal Today 212:75–80
51. Shaban M, Ahmed AM, Shehata N et al (2019) Ni-doped and Ni/Cr co-doped TiO_2 nanotubes for enhancement of photocatalytic degradation of methylene blue. J Colloid Interface Sci 555:31–41
52. Li YX, Ma GF, Peng SQ et al (2008) Boron and nitrogen co-doped titania with enhanced visible-light photocatalytic activity for hydrogen evolution. Appl Surf Sci 254(21):6831–6836
53. Khalilian H, Behpour M, Atouf V et al (2015) Immobilization of S, N-codoped TiO_2 nanoparticles on glass beads for photocatalytic degradation of methyl orange by fixed bed photoreactor under visible and sunlight irradiation. Sol Energy 112:239–245
54. Divya Lakshmi KV, Siva Rao T, Swathi Padmaja J et al (2019) Structure, photocatalytic and antibacterial activity study of Meso porous Ni and S co-doped TiO_2 nano material under visible light irradiation. Chin J Chem Eng 27(7):1630–1641
55. Hoang S, Guo SW, Mullins CB (2012) Coincorporation of N and Ta into TiO_2 nanowires for visible light driven photoelectrochemical water oxidation. J Phys Chem C 116(44):23283–23290
56. Wang W, Tadé MO, Shao ZP (2018) Nitrogen-doped simple and complex oxides for photocatalysis: a review. Prog Mater Sci 92:33–63
57. Basavarajappa PS, Patil SB, Ganganagappa N et al (2020) Recent progress in metal-doped TiO_2, non-metal doped/codoped TiO_2 and TiO_2 nanostructured hybrids for enhanced photocatalysis. Int J Hydrog Energy 45(13):7764–7778
58. Asahi R, Morikawa T, Ohwaki T et al (2001) Visible-light photocatalysis in nitrogen-doped titanium oxides. Science 293(5528):269–271
59. Ma Y, Wang X, Jia Y et al (2014) Titanium dioxide-based nanomaterials for photocatalytic fuel generations. Chem Rev 114(19):9987–10043
60. Ullattil SG, Narendranath SB, Pillai SC et al (2018) Black TiO_2 nanomaterials: a review of recent advances. Chem Eng J 343:708–736
61. Kumaravel V, Mathew S, Bartlett J et al (2019) Photocatalytic hydrogen production using metal doped TiO_2: a review of recent advances. Appl Catal B Environ 244:1021–1064
62. Chen DJ, Cheng YL, Zhou N et al (2020) Photocatalytic degradation of organic pollutants using TiO_2-based photocatalysts: a review. J Clean Prod 268:121725
63. Xiong Z, Lei Z, Li YZ et al (2018) A review on modification of facet-engineered TiO_2 for photocatalytic CO_2 reduction. J Photochem Photobiol C Photochem Rev 36:24–47
64. Naldoni A, Altomare M, Zoppellaro G et al (2019) Photocatalysis with reduced TiO_2: from black TiO_2 to cocatalyst-free hydrogen production. ACS Catal 9(1):345–364
65. Zhang YC, Yang M, Zhang GS et al (2013) HNO_3-involved one-step low temperature solvothermal synthesis of N-doped TiO_2 nanocrystals for efficient photocatalytic reduction of Cr(VI) in water. Appl Catal B Environ 142–143:249–258
66. Sanchez-Martinez A, Ceballos-Sanchez O, Koop-Santa C et al (2018) N-doped TiO_2 nanoparticles obtained by a facile coprecipitation method at low temperature. Ceram Int 44(5):5273–5283

67. Singha K, Ghosh SC, Panda AB (2019) N-doped yellow TiO_2 hollow sphere-mediated visible-light-driven efficient esterification of alcohol and N-hydroxyimides to active esters. Chem Asian J 14(18):3205–3212
68. Marques J, Gomes TD, Forte MA et al (2019) A new route for the synthesis of highly-active N-doped TiO_2 nanoparticles for visible light photocatalysis using urea as nitrogen precursor. Catal Today 326:36–45
69. Kalantari K, Kalbasi M, Sohrabi M et al (2016) Synthesis and characterization of N-doped TiO_2 nanoparticles and their application in photocatalytic oxidation of dibenzothiophene under visible light. Ceram Int 42(13):14834–14842
70. Di Camillo D, Ruggieri F, Santucci S et al (2012) N-doped TiO_2 nanofibers deposited by electrospinning. J Phys Chem C 116(34):18427–18431
71. Livraghi S, Paganini MC, Giamello E et al (2006) Origin of photoactivity of nitrogen-doped titanium dioxide under visible light. J Am Chem Soc 128(49):15666–15671
72. Katoueizadeh E, Zebarjad SM, Janghorban K (2018) Synthesis and enhanced visible-light activity of N-doped TiO_2 nanoadditives applied over cotton textiles. J Mater Res Technol 7(3):204–211
73. Mrowetz M, Balcerski W, Colussi AJ et al (2004) Oxidative power of nitrogen-doped TiO_2 photocatalysts under visible illumination. J Phys Chem B 108(45):17269–17273
74. Mbouopda AP, Acayanka E, Boyom-Tatchemo FW et al (2018) New-route synthesis of N-doped TiO_2 via exposing the $TiCl_3$ precursor to non-thermal quenched plasma at various times. Mater Chem Phys 206:224–231
75. Jia TK, Fu F, Yu DS et al (2018) Facile synthesis and characterization of N-doped TiO_2/C nanocomposites with enhanced visible-light photocatalytic performance. Appl Surf Sci 430:438–447
76. He HY (2010) Solvothermal synthesis and photocatalytic activity of S-doped TiO_2 and TiS_2 powders. Res Chem Intermed 36(2):155–161
77. Tan XF, Qin GD, Cheng G et al (2020) Oxygen vacancies enhance photocatalytic removal of NO over an N-doped TiO_2 catalyst. Catal Sci Technol 10(20):6923–6934
78. Cheng XW, Yu XJ, Xing ZP et al (2012) Enhanced photocatalytic activity of nitrogen doped TiO_2 anatase nano-particle under simulated sunlight irradiation. Energy Procedia 16:598–605
79. Asahi R, Morikawa T, Irie H et al (2014) Nitrogen-doped titanium dioxide as visible-light-sensitive photocatalyst: designs, developments, and prospects. Chem Rev 114(19):9824–9852
80. Morikawa T, Asahi R, Ohwaki T et al (2001) Band-gap narrowing of titanium dioxide by nitrogen doping. Jpn J Appl Phys 40:L561–L563
81. Wu ZB, Dong F, Zhao WR et al (2008) Visible light induced electron transfer process over nitrogen doped TiO_2 nanocrystals prepared by oxidation of titanium nitride. J Hazard Mater 157(1):57–63
82. Xia L, Yang Y, Cao Y et al (2019) Porous N-doped TiO_2 nanotubes arrays by reverse oxidation of TiN and their visible-light photocatalytic activity. Surf Coat Technol 365:237–241
83. Irie H, Watanabe Y, Hashimoto K (2003) Nitrogen-concentration dependence on photocatalytic activity of $TiO_{2-x}N_x$ powders. J Phys Chem B 107(23):5483–5486
84. Rengifo-Herrera JA, Mielczarski E, Mielczarski J et al (2008) Escherichia coli inactivation by N, S co-doped commercial TiO_2 powders under UV and visible light. Appl Catal B Environ 84(3–4):448–456
85. Fang XM, Zhang ZG, Chen QL et al (2007) Dependence of nitrogen doping on TiO_2 precursor annealed under NH_3 flow. J Solid State Chem 180(4):1325–1332
86. Huang J, Dou L, Li J et al (2021) Excellent visible light responsive photocatalytic behavior of N-doped TiO_2 toward decontamination of organic pollutants. J Hazard Mater 403:123857
87. Yin S, Yamaki H, Komatsu M et al (2003) Preparation of nitrogen-doped titania with high visible light induced photocatalytic activity by mechanochemical reaction of titania and hexamethylenetetramine. J Mater Chem 13(12):2996
88. Vasu K, Sreedhara MB, Ghatak J et al (2016) Atomic layer deposition of p-type epitaxial thin films of undoped and N-doped anatase TiO_2. ACS Appl Mater Interfaces 8(12):7897–7901
89. Liu G, Yang HG, Wang X et al (2009) Visible light responsive nitrogen doped anatase TiO_2 sheets with dominant 001 facets derived from TiN. J Am Chem Soc 131(36):12868–12869
90. Nakada A, Nishioka S, Vequizo JJM et al (2017) Solar-driven Z-scheme water splitting using tantalum/nitrogen co-doped rutile titania nanorod as an oxygen evolution photocatalyst. J Mater Chem A 5(23):11710–11719
91. Nukumizu K, Nunoshige J, Takata T et al (2003) $TiN_xO_yF_z$ as a stable photocatalyst for water oxidation in visible light (<570 nm). Chem Lett 32(2):196–197
92. Maeda K, Shimodaira Y, Lee B et al (2007) Studies on $TiN_xO_yF_z$ as a visible-light-responsive photocatalyst. J Phys Chem C 111(49):18264–18270
93. Zong X, Xing Z, Yu H et al (2011) Photocatalytic water oxidation on F, N co-doped TiO2 with dominant exposed 001 facets under visible light. Chem Commun Camb Engl 47(42):11742–11744
94. Miyoshi A, Vequizo JJM, Nishioka S et al (2018) Nitrogen/fluorine-codoped rutile titania as a stable oxygen-evolution photocatalyst for solar-driven Z-scheme water splitting. Sustain Energy Fuels 2(9):2025–2035
95. Liu G, Zhao Y, Sun C et al (2008) Synergistic effects of B/N doping on the visible-light photocatalytic activity of mesoporous TiO_2. Angew Chem Int Ed Engl 47(24):4516–4520
96. Hong XX, Tan J, Zhu HZ et al (2019) Control of spatially homogeneous distribution of heteroatoms to produce red TiO_2 photocatalyst for visible-light photocatalytic water splitting. Chem Eur J 25(7):1787–1794
97. Wu TT, Niu P, Yang YQ et al (2019) Homogeneous doping of substitutional nitrogen/carbon in TiO_2 plates for visible light photocatalytic water oxidation. Adv Funct Mater 29(25):1901943
98. Zheng P, Wu HJ, Guo JL et al (2014) P-N co-doping induced structural recovery of TiO_2 for overall water splitting under visible light irradiation. J Alloy Compd 615:79–83
99. Wang F, Ma ZZ, Ban PP et al (2017) C, N and S codoped rutile TiO_2 nanorods for enhanced visible-light photocatalytic activity. Mater Lett 195:143–146
100. Liu G, Wang LZ, Yang HG et al (2010) Titania-based photocatalysts-crystal growth, doping and heterostructuring. J Mater Chem 20(5):831–843
101. Ihara T, Miyoshi M, Iriyama Y et al (2003) Visible-light-active titanium oxide photocatalyst realized by an oxygen-deficient structure and by nitrogen doping. Appl Catal B Environ 42(4):403–409
102. Shin CH, Bugli G, Djega-Mariadassou G (1991) Preparation and characterization of titanium oxynitrides with high specific surface areas. J Solid State Chem 95(1):145–155
103. Zhao B, Wang X, Zhang YZ et al (2019) Synergism of oxygen vacancies, Ti^{3+} and N dopants on the visible-light photocatalytic activity of N-doped TiO_2. J Photochem Photobiol A Chem 382:111928
104. Powell MJ, Dunnill CW, Parkin IP (2014) N-doped TiO_2 visible light photocatalyst films via a sol-gel route using TMEDA as the nitrogen source. J Photochem Photobiol A Chem 281:27–34
105. Serpone N (2006) Is the band gap of pristine TiO_2 narrowed by anion- and cation-doping of titanium dioxide in second-generation photocatalysts? J Phys Chem B 110(48):24287–24293

106. Dong BB, Cui JY, Liu TF et al (2018) Development of novel perovskite-like oxide photocatalyst $LiCuTa_3O_9$ with dual functions of water reduction and oxidation under visible light irradiation. Adv Energy Mater 8(35):1801660
107. Tachikawa T, Takai Y, Tojo S et al (2006) Visible light-induced degradation of ethylene glycol on nitrogen-doped TiO_2 powders. J Phys Chem B 110(26):13158–13165
108. Katoh R, Furube A, Yamanaka KI et al (2010) Charge separation and trapping in N-doped TiO_2 photocatalysts: a time-resolved microwave conductivity study. J Phys Chem Lett 1(22):3261–3265
109. Yamanaka KI, Morikawa T (2012) Charge-carrier dynamics in nitrogen-doped TiO_2 powder studied by femtosecond time-resolved diffuse reflectance spectroscopy. J Phys Chem C 116(1):1286–1292
110. Chen YJ, Luo X, Luo Y et al (2019) Efficient charge carrier separation in l-alanine acids derived N-TiO_2 nanospheres: the role of oxygen vacancies in tetrahedral Ti^{4+} sites. Nanomaterials 9(5):698
111. Tang JW, Cowan AJ, Durrant JR et al (2011) Mechanism of O_2 production from water splitting: nature of charge carriers in nitrogen doped nanocrystalline TiO_2 films and factors limiting O_2 production. J Phys Chem C 115(7):3143–3150
112. Zhang N, Gao C, Xiong YJ (2019) Defect engineering: a versatile tool for tuning the activation of key molecules in photocatalytic reactions. J Energy Chem 37:43–57
113. Salarian AA, Hami Z, Mirzaei N et al (2016) N-doped TiO_2 nanosheets for photocatalytic degradation and mineralization of diazinon under simulated solar irradiation: optimization and modeling using a response surface methodology. J Mol Liq 220:183–191
114. Makropoulou T, Panagiotopoulou P, Venieri D (2018) N-doped TiO_2 photocatalysts for bacterial inactivation in water. J Chem Technol Biotechnol 93(9):2518–2526
115. Horovitz I, Avisar D, Luster E et al (2018) MS_2 bacteriophage inactivation using a N-doped TiO_2-coated photocatalytic membrane reactor: influence of water-quality parameters. Chem Eng J 354:995–1006
116. Bjelajac A, Kopač D, Fecant A et al (2020) Micro-kinetic modelling of photocatalytic CO_2 reduction over undoped and N-doped TiO_2. Catal Sci Technol 10(6):1688–1698
117. Akple MS, Low J, Qin ZY et al (2015) Nitrogen-doped TiO_2 microsheets with enhanced visible light photocatalytic activity for CO_2 reduction. Chin J Catal 36(12):2127–2134
118. Zhang ZG, Huang ZF, Cheng XD et al (2015) Product selectivity of visible-light photocatalytic reduction of carbon dioxide using titanium dioxide doped by different nitrogen-sources. Appl Surf Sci 355:45–51
119. Yun HJ, Lee DM, Yu S et al (2013) Effect of valence band energy on the photocatalytic performance of N-doped TiO_2 for the production of O_2 via the oxidation of water by visible light. J Mol Catal A Chem 378:221–226
120. Lee M, Yun HJ, Yu S et al (2014) Enhancement in photocatalytic oxygen evolution via water oxidation under visible light on nitrogen-doped TiO_2 nanorods with dominant reactive 102 facets. Catal Commun 43:11–15
121. Yuan J, Chen MX, Shi JW et al (2006) Preparations and photocatalytic hydrogen evolution of N-doped TiO_2 from urea and titanium tetrachloride. Int J Hydrog Energy 31(10):1326–1331
122. Sun S, Gao P, Yang Y et al (2016) N-doped TiO_2 nanobelts with coexposed (001) and (101) facets and their highly efficient visible-light-driven photocatalytic hydrogen production. ACS Appl Mater Interfaces 8(28):18126–18131
123. Wang J, Fan C, Ren Z et al (2014) N-doped TiO_2/C nanocomposites and N-doped TiO_2 synthesised at different thermal treatment temperatures with the same hydrothermal precursor. Dalton Trans 43(36):13783–13791
124. Yu L, Yang XF, He J et al (2015) One-step hydrothermal method to prepare nitrogen and lanthanum co-doped TiO2 nanocrystals with exposed 001 facets and study on their photocatalytic activities in visible light. J Alloy Compd 637:308–314
125. Shi JW, Liu C, Ai HY et al (2015) One step to synthesize the nanocomposites of graphene nanosheets and N-doped titania nanoplates with exposed 001 facets for enhanced visible-light photocatalytic activity. J Nanopart Res 17(5):1–10
126. Japa M, Tantraviwat D, Phasayavan W et al (2021) Simple preparation of nitrogen-doped TiO_2 and its performance in selective oxidation of benzyl alcohol and benzylamine under visible light. Colloids Surf A Physicochem Eng Asp 610:125743
127. Xu G, Zhang Y, Peng DD et al (2021) Nitrogen-doped mixed-phase TiO_2 with controllable phase junction as superior visible-light photocatalyst for selective oxidation of cyclohexane. Appl Surf Sci 536:147953
128. May Ix LA, Estrella-González A, Díaz CS et al (2020) Effective electron-hole separation over N-doped TiO_2 materials for improved photocatalytic reduction of 4-nitrophenol using visible light. J Chem Technol Biotechnol 95(10):2694–2706
129. Inoue T, Fujishima A, Konishi S et al (1979) Photoelectrocatalytic reduction of carbon dioxide in aqueous suspensions of semiconductor powders. Nature 277(5698):637–638
130. Maeda K, Lee B, Lu DL et al (2009) Physicochemical effects on photocatalytic water oxidation by titanium fluorooxynitride powder under visible light. Chem Mater 21(11):2286–2291

Fuxiang Zhang a full professor of physical chemistry, fellow of Royal Society of Chemistry (FRSC), earned his bachelor's degree (1999), Ph.D. (2004) and then worked as the faculty in Nankai University. During 2007–2011, he pursued postdoctoral research at the University of Pierre & Marie Curie, in France and at the University of Tokyo, separately. Since October 2011, he has been working at Dalian Institute of Chemical Physics (DICP) to develop novel photocatalytic materials with wide visible light utilization for promising solar-to-chemical conversion.